Complex Formation of Immunoglobulin Superfamily Molecules Side-IV and Beat-IIb Regulates Synaptic Specificity in the *Drosophila* Visual System

Jiro Osaka[1], Arisa Ishii[1], Xu Wang[1], Satoko Hakeda-Suzuki[1,2], Riku Iwanaga[1], Hinata Kawamura[1], Takashi Suzuki[1*]

1. School of Life Science and Technology, Tokyo Institute of Technology, Yokohama, 226-8501, Japan
2. Research Initiatives and Promotion Organization, Yokohama National University, Yokohama, 240-8501, Japan

*: Corresponding author.
suzukit@bio.titech.ac.jp (T.S.)

SUMMARY

Neurons express many cell surface proteins as mutually binding "key-lock molecules" that can create synapses. However, the molecular mechanisms of how neurons make synapses only with preferred targets are not completely understood. Here we identified Side-IV and Beat-IIb, belonging to the *Drosophila* immunoglobulin superfamily, as a new key-lock combination capable of inducing synapse formation. Side-IV interaction with Beat-IIb transduces bifurcated signaling to Side-IV's co-receptor, Kirre, and a synaptic scaffold protein, Dsyd-1. Localization and genetic interaction analyses revealed that Side-IV localizes subcellularly at synapse formations defined by Beat-IIa/b and anchors Dsyd-1. Our data demonstrate that a complex made up of Side-IV, Beat-IIb, Kirre, and Dsyd-1 not only narrows neuronal binding specificity but also recruits synapse formation factors Kirre and Dsyd-1 to restrict synapse formation loci and inhibit miswiring. We propose a mechanism by which key-lock molecules set a hierarchy of preference among neuronal pairs in a complex circuit in vivo.

Keywords: synaptic specificity, synapse formation, key-lock molecules, transmembrane clustering, subcellular localization, Beat and Side proteins, irre cell recognition module, Dsyd-1-Liprin-α

INTRODUCTION

All neurons can potentially form synapses with many other neurons, but still demonstrate specificity in synapse partner selection.[1-4] During development, neurons stochastically extend filopodia, searching for synaptic partners.[5-7] Synaptogenesis begins only when filopodia find a synaptic partner through specific molecular interactions.[2,5] By the study

of synapse formation in cultured cells, several cell surface proteins were found to have "key-lock molecules" that can induce synapse formation.[8] In vivo studies have shown that neurons have the capability to form a constant number of synapses indiscriminately; however, they rank target synapses according to a preferred order.[3,4] The molecular mechanisms that drive synaptic preferences and specificity have not been fully explored.

The *Drosophila* visual system consists of a compound eye and four optic ganglia, compactly composed of about 200 diverse neurons with well-documented connections.[9,10] In addition, single-cell analyses in the last few years have revealed cell-type and time-specific gene expression profiles of the *Drosophila* visual system, which have been compiled into a database such as Gene Expression Omnibus.[11-15] This makes the *Drosophila* visual system an ideal model for connectome and transcriptome-based analyses. Several transmembrane protein pairs with binding interactions have been reported to be expressed between synaptic partners.[13,16-18] The most studied is the DIP-Dpr families of the immunoglobulin superfamily (IgSF), which forms heterophilic or homophilic interaction networks.[16,19] In recent years, it has been shown that DIP-Dpr protein interactions are involved in neural connections, axon guidance, and cell death signaling.[3,17,18,20-24] Another member of IgSF, the Beat-Side families, have similar properties to DIP-Dpr, although its function is less well understood. Therefore, we considered the Beat-Side families as a candidate for the molecules involved in neural circuit formation.

Both *beaten path Ia* (*beat-Ia*) and *sidestep* (*side*) were identified by the genetic screening of mutants showing abnormal axon guidance in neuromuscular junctions (NMJ).[25-27] The *beat-Ia* and *side* mutants had similar phenotypes and were shown to interact genetically and biochemically.[16,28,29] Genomic and interactome analyses revealed

that *beat-Ia* and *side* have 14 and 8 paralogs, respectively, with a heterophilic interaction network.[16,29-32] Furthermore, single-cell RNAseq data showed that Beat-Side families are expressed in a cell-specific manner throughout the nervous system.[11,13] Although several works have reported the function of Beat-Ia/Side interaction in NMJ, motor function, and leg nerve development,[28,33-35] the functions of other Beat-Side families are still elusive, especially in the central nervous system.

In the present study, we report a new key-lock combination in synaptic specificity, Side-IV and Beat-IIb. Overexpression of *side-IV* can induce synapses in the R7 photoreceptor in *Drosophila*. Triggered by *trans*-interaction with Side-IV, Beat-IIb made a cluster complex that can transduce bifurcated signaling to induce synapses with its co-receptor, Kirre, and a synaptic scaffold protein, Dsyd-1. Surprisingly, in *side-IV* loss of function analysis, against our intuitive guess, we saw more ectopic synapse formation in the distal part of lamina monopolar neurons. Combining loss-of-function analyses and subcellular protein localization analyses, we demonstrated that the newly characterized Side-IV/Beat-IIb/Kirre/Dsyd-1 complex has two functions. One is to narrow neuronal binding specificity via Side-IV/Beat-IIb extracellular interactions. The second is to recruit synapse formation factors Kirre and Dsyd-1 to restrict synapse formation loci and inhibit miswiring. These two functions can explain how redundant key-lock molecules can rank preferred interactions among neuronal pairs and accomplish synaptic specificity in a complex circuit.

RESULTS

Side-IV and Beat-IIb are a New Key-Lock Combination for Synaptic Induction

To identify a new key-lock molecule, we focused on the function of the Beat-Side families. Photoreceptor R7 projects its axons to the medulla and mainly synapses on the dendrite of Dm8 in the M4–M6 layer.[10,36] The presynaptic structure of R7 is limited to the M4–M6 layer.[6,37] By utilizing synaptic tagging with recombination (STaR),[37] which can label the active zone protein Bruchpilot (Brp) in a cell-specific manner, we specifically visualized R7's presynaptic structures with R7-specific FLPase 20C11-FLP (Figure 1A).

Beat-Side family members were either knocked down (Figures S1A and B) or overexpressed (Figures S1C and D) in R7. We found that ectopic synapses were induced in the M1–M3 layer of R7 by overexpression of *side-IV* (Figures 1B and B', yellow allows, and S1C). In addition, some axons overshot toward the M10 layer (Figures 1B and B", yellow arrowheads). These phenotypes suggested that R7 was miswired around M1–M3 and M10 layers other than M4–M6 due to expression of *side-IV*. Endogenous tags of Side-IV revealed R7 doesn't endogenously expresses *side-IV* (Figures S1E–I'). Since Side-IV biochemically interacts with Beat-IIa and Beat-IIb,[16,29] we tested if Side-IV-Beat-IIa/b interactions were responsible for the miswiring phenotypes. Both synaptic induction and overshoot phenotypes generated by *side-IV* overexpression were significantly suppressed in a *beat-IIa* or *beat-IIb* mutant background (Figures 1C–G). An endogenous Beat-IIb marker[38] showed layer-specific expression in the M1–M2 and M9–M10 layers where miswiring phenotypes occurred (Figures 1H–I). Furthermore, we found that the Beat-IIb signals became punctate when *side-IV* was expressed (Figures 1J–K"), and presynaptic Brp puncta were induced adjacently (Figures 1K' and K", yellow arrows). The punctate signal suggested clustering transmembrane proteins, a common phenomenon seen with other synapse-organizing molecules.[39] The concurrent

visualization of Side-IV, Beat-IIb, and Brp also revealed clustered signals of Side-IV, about 70% of which co-localized with Beat-IIb clusters (Figures 1L–L"). Furthermore, about 70% of Side-IV/Beat-IIb clustered signals co-localized with ectopic synapses (Figures 1L−L", yellow arrows). These data indicated that Side-IV induced Beat-IIb clustering, and that this cluster complex induced synapse (Figure 1M). We therefore have identified Side-IV/Beat-IIb as a new key-lock combination capable of inducing synapses by establishing cluster complexes.

Side-IV Transduces Signals Both by its Co-Receptors and the Cytoplasmic Domain to Induce Synapses

To uncover the mechanism of synaptic induction by Side-IV, we investigated the impact of each domain. Side-IV has five extracellular Ig domains (Ig1–5), a fibronectin type III domain (FnIII), and a cytoplasmic domain (Cyto) with a PDZ-binding motif (PDZb) (Figure 2A). We constructed domain-deficient variants (Figure S2A) and chimeras of Side-IV with a non-functional membrane protein, mCD8 (Figures 2A and B). With these constructs, we analyzed the Side-IV/Beat-IIb clustering and ectopic synapse/overshoot induction phenotypes in R7 (Figures 2 and S2B–K). We found that Side-IV could not induce synapse without an extracellular Ig domain (Figures S2B–E, and I). In *Drosophila* S2 cells, cell aggregations were formed via *trans*-interactions when *side-IV* expressing cells were mixed with *beat-IIb* expressing cells (Figures S2L–L", yellow dotted lines). The cell aggregations were not formed by Side-IV $^{\Delta Ig1}$ or Side-IV $^{\Delta Ig1–5}$ (Figures S2M–O"), indicating that the Ig domain is necessary for *trans*-interaction. The chimeric protein with the extracellular domain of Side-IV fused with the transmembrane and cytoplasmic domains of mCD8 (Side-IV^{Ecto}::mCD8$^{TM+Cyto}$) showed a similar degree of synapse

144 induction as Side-IV $^{\Delta Cyto}$ (Figures 2E–F''', and H–K), suggesting that the transmembrane
145 domain of Side-IV is not important for synaptic induction. On the other hand, the chimeric
146 protein with the extracellular domain of Side-IV fused with mCD8 and the FnIII domain
147 deleted (Side-IV $^{Ecto\Delta FnIII}$::mCD8) showed no cluster signal in the M1–M3 layer of R7 and
148 failed to induce synapses (Figures 2G–K). This indicates that the FnIII domain is essential
149 for Side-IV clustering. *Side-IV$^{Ecto\Delta FnIII}$::mCD8* expressing cells demonstrate strong cell
150 aggregation with *beat-IIb* expressing cells, to a similar degree as *side-IV^{FL}* (Figures S2P–
151 Q). This indicates that the chimera has a strong affinity for Beat-IIb but has lost clustering
152 ability. These data suggest that the Ig domains are important for *trans*-interaction with
153 Beat-IIb, and the FnIII domains are important for Side-IV clustering; both are required to
154 establish the Side-IV/Beat-IIb clustering complex, which is crucial for synaptic induction.
155 Introducing Nrxs-Nlgs interaction induced synapse formation in M1–M3, but
156 the homophilic interactions of epithelial cadherins or human-derived sidekick cell
157 adhesion molecule 2 (SDK2) did not (Figure S3). This indicates that increased affinity
158 between R7 and postsynaptic neurons[40] is not sufficient for synaptic induction. Therefore,
159 we hypothesized that the Side-IV/Beat-IIb cluster complex could transduce signals. Side-
160 IV could induce synapses without the cytoplasmic domain (Figures 2E–E''', and J). Side-
161 IV may transduce signal via its co-receptors. The synaptic induction phenotype of Side-
162 IV$^{\Delta Cyto}$ or Side-IV$^{\Delta PDZb}$ was much weaker than that of full-length Side-IV (Figures 2D–
163 E''', and J; Figures S2C, G–I), indicating that signaling through the PDZ-binding motif
164 also contributed to synaptic induction. Side-IV may have two distinct signaling pathways
165 transduced by its co-receptors and the cytoplasmic domain. Taken together, these data
166 show that the extracellular Ig and FnIII domains of Side-IV are essential for establishing

the Side-IV/Beat-IIb cluster complex, and the cytoplasmic domain of Side-IV and/or its co-receptors may transduce signals for synapse organization.

Kirre Can Form a Complex with Side-IV with the Extracellular Domain as a Co-Receptor

To identify the co-receptor of Side-IV, we searched for transmembrane proteins that can enhance Side-IV signaling. The immunoglobulin superfamily protein Kirre[41] can enhance Side-IV's phenotypes (Figures 3A–F). Kirre expression doubled the Side-IV overshoot phenotype, while Kirre itself could not induce an overshoot at all, indicating that the enhancement is not additive, but synergistic (Figure 3F). By analyzing the overshoot phenotype, we tested the impact of the cytoplasmic domains on the synergistic effects (Figures 3G–P). Side-IV and Kirre had little synergy when each lacked a cytoplasmic domain (Figures 3O and P). On the other hand, they were strongly synergistic when either cytoplasmic domain remained (Figures 3L, N, and P). This suggests that Kirre can enhance Side-IV signaling, through the cytoplasmic domains, as a co-receptor.

If Kirre works as a co-receptor of Side-IV, the two proteins would likely form a Side-IV/Kirre complex. As predicted, Side-IV co-immunoprecipitated with Kirre, and *vice versa* (Figure S4A). Since Side-IV and Kirre did not form cell aggregation via *trans*-interactions (Figures S4B–D), they may form a complex by their *cis*-interaction. In *Drosophila* S2 cells, Flamingo polarity protein accumulates at cell contact surfaces and can recruit transmembrane proteins Vang, Frizzled, and Gogo by *cis*-interactions.[42,43] Using S2 cells, we assessed the *cis*-interaction between Side-IV and Kirre. Homophilic self-interaction of Kirre causes Kirre-transfected S2 cells to form aggregates, often accumulating at sites of cell-cell contact (Figures 3Q and Q'). We noted Side-IV co-

accumulation with Kirre (Figures 3Q" and R). Since Side-IV co-accumulation did not occur when *cadE*-expressing cells aggregated via their homophilic interactions (Figures 3S–T), the effect was Kirre-specific. These data suggest that Side-IV and Kirre form a complex at the cell membrane through their *cis*-interaction. Furthermore, the accumulation requires Side-IV's extracellular domain but not its cytoplasmic domain (Figures 3U and V). This result was consistent with the domain requirement for synergy between Side-IV and Kirre in the overshoot phenotype (Figure S4 E–M). These data suggest that Kirre may work as a co-receptor of Side-IV, and that they form a Side-IV/Kirre complex established by *cis* interaction through their extracellular domains.

The Cytoplasmic Domain of Side-IV May Establish a Dsyd-1-Liprin-α Complex that Functions Downstream

The synaptic induction of Side-IV$^{\Delta Cyto}$ suggests that signaling through the cytoplasmic domain is also functionally required for signaling. To identify the downstream signaling targets of Side-IV, we searched for synapse related molecules necessary for Side-IV synaptic induction. By the RNAi approach, we found that knocking down *dsyd-1* or *liprin-α* could significantly suppress synaptic induction by *side-IV* overexpression in R7 (Figures 4A–F), suggesting that Dsyd-1 and Liprin-α work downstream of Side-IV.

Using S2 cells, we analyzed the co-localization of Side-IV with Dsyd-1 and Liprin-α (Figures 4G–L). Side-IV showed substantial co-localization with Dsyd-1 (Figures 4G and I). Since Dsyd-1 has a PDZ domain that interacts with synapse-organizing molecules such as Nrx-1,[44] we hypothesized that Side-IV interacts with Dsyd-1 through Side-IV's PDZ-binding motif. The co-localization index between Side-IV and Dsyd-1 decreased by almost half in the absence of Side-IV's PDZ-binding motif (Figures

4H–I), indicating its necessity for the Side-IV/Dsyd-1 interaction. Although Side-IV and Liprin-α did not show strong co-localization, their co-localization index almost doubled when *dsyd-1* was also expressed in the S2 cells (Figures 4J–L). This indicates that Side-IV can form a complex with Liprin-α through Dsyd-1. These data suggest that the PDZ-binding motif of Side-IV interacts with Dsyd-1, and establish Dsyd-1/Liprin-α as a complex important for active zone formation.[44,45]

To validate the idea that Dsyd-1 and Liprin-α work downstream of the cytoplasmic domain of Side-IV, we utilized Side-IV$^{\Delta Cyto}$, which cannot transduce cytoplasmic signaling. Knockdown of *dsyd-1* suppressed synaptic induction by Side-IV^{FL}, but not Side-IV$^{\Delta Cyto}$ (Figure 4M), indicating that Dsyd-1 acts exclusively on signaling through the Side-IV's cytoplasmic domain. On the other hand, knockdown of *liprin-α* suppressed synaptic induction by both Side-IV^{FL} and Side-IV$^{\Delta Cyto}$ (Figure 4M). This indicates that Liprin-α affects signaling both through the Side-IV's cytoplasmic domain and the co-receptor(s). The knockdown of *kirre* suppressed synaptic induction by Side-IV$^{\Delta Cyto}$, but not Side-IV^{FL} (Figure 4M), indicating that Kirre affects signaling independent of the cytoplasmic domain. These data indicate that Side-IV forms a signaling complex with Kirre as a co-receptor, and additionally with Dsyd-1/Liprin-α downstream of the cytoplasmic domain (Figure 4N).

***side-IV* and *side-VII* are Required for Synapse Formation of L2 Neurons Restricted in the Proximal Region**

By toggled expression experiments of *side-IV* in R7, we found that Side-IV/Beat-IIb is a new key-lock combination for synaptic induction at the presynapse of R7. To analyze

their endogenous function, we searched for synaptic partners where Side-IV/Beat-IIb interaction functions by utilizing single-cell RNAseq data in the *Drosophila* visual system.[11,17] The Side-IV/Beat-IIa/b and Side-VII/Beat-IV interactions were predicted between L2 and L4 neurons (Figures 5A and B).[11,17] Furthermore, endogenous tags of Side-IV showed signals in the M2 layer (Figures S1F and F'), indicating that L2 expressed *side-IV*. Although there are five subtypes of lamina neurons, only L2 and L4 make reciprocal synapses restricted to the proximal region of the lamina (Figures 5A, C, and C').[46] We generated *side-IV* or *side-VII* mutants (see Methods) and analyzed the function of Beat-Side interactions for the synapse formation (Figures 5C–H).

Despite Side-IV's strong synapse-organizing ability in R7, the *side-IV* mutant did not show any decrease in synapse number in the proximal region (Figures 5C–D', and G). Potentially, the loss of synapse-organizing molecules did not result in synaptic loss because of molecular redundancy[47,48]; disrupting a few genes may not be sufficient for decreasing synapse numbers. At least ten transmembrane interactions were predicted between L2 and L4,[13] indicating that these synaptic connections may have high molecular redundancy. However, the *side-IV* mutant showed ectopic synapse formation in the distal region (Figures 5C–D', and H), similar to those reported in the *dip-β* mutant.[3] We conducted rescue experiments of *side-IV* and found the Side-IV ^{FL} could rescue the phenotype completely while Side-IV $^{\Delta Cyto}$ could partially (Figures. S5A–D), indicating that regaining the physical strength of cell-cell contact is not sufficient, but cytoplasmic signaling is also important. The *side-VII* mutants also showed ectopic synapse formation in the distal region, which was significantly enhanced in the *side-IV* / *side-VII* double mutants (Figures 5E–H). Knockdown of *side-IV* or *side-VII*, specifically in L2, resulted in ectopic synapse formation in the distal region, indicating that *side-IV* and *side-VII* are

required in L2 (Figures S5E–H). Furthermore, downregulation of *beat-IIa/b* or *beat-IV* phenocopied the ectopic synapse formation in the distal region (Figures S5I–P). To assess which lamina neuron actually induced the ectopic synapse formation by diminishing Beat-Side interactions, we analyzed the synapse of each subtype of lamina neuron in *side-IV* / *side-VII* double mutant flies. L2 showed ectopic synapse formation in the distal region (Figures 5I–L), whereas other subtypes did not (Figure S6). These data indicate that Side-IV/Beat-IIa/b and Side-VII/Beat-IV interactions are necessary for proper synapse formation, restricted to the proximal region, of L2. Side-IV and Side-VII may regulate the synaptic specificity of L2 by indicating the location of synapse formation.

Side-IV and Side-VII Demonstrate Beats-Dependent Subcellular Localization to the Proximal Region

If Side-IV and Side-VII determine the location of synapse formation of L2, both should localize to the proximal region where presynaptic structures are formed. We analyzed the endogenous localization of Side-IV and Side-VII with FLPase-based cell-specific tags (Figure S1E). The co-localization of Side-IV, Side-VII, and Brp at 72 hours after puparium formation (APF) revealed that Side-IV and Side-VII localization was restricted to the proximal region (Figures 6A–A'''). Both *side-IV* and *side-VII* were expressed in L2 neurons, from developmental to adult stages (Figure S7). At the 72 hour APF and adult stages, endogenous Side-IV and Side-VII showed subcellular localization restricted to the proximal region (Figures S7C–D' and G–H'). This characteristic subcellular localization was also observed when the GFP-tagged *side-IV* or *side-VII* was expressed in L2 neurons (Figures 6B–C'). Since the dendritic arbors of the L2 neuron are uniform from the distal to proximal regions,[49,50] we speculated that the subcellular localization of Side-IV and

Side-VII is regulated in a non-cell-autonomous manner. We hypothesized that Beats expressed in L4 might define the subcellular localization of Sides.

We analyzed the localization dependency of Side-IV and Side-VII on Beat-IIa/b and Beat-IV, respectively (Figures 6D–M). In the wild type, Side-IV localized from the proximal to the distal region at 48 hours APF (Figures 6D and D'). Subcellular localization to the proximal region was observed at 72 hours APF (Figures 6F and F'). With downregulated *beat-IIa/b*, Side-IV localized similarly to the wild type condition at 48 hours APF (Figures 6E and E'). However, it failed to localize to the proximal region at 72 hours APF (Figures 6G–H). The localization of Side-VII in the wild type was similar to that of Side-IV, appearing throughout the lamina at 48 hours APF (Figures 6I and I') and only the proximal region at 72 hours APF (Figures 6L and L'). Similar to the impact of *beat-IIa/b* downregulation on Side-IV localization, the downregulation of *beat-IV* did not affect Side-VII localization at 48 hours APF (Figures 6J and J') but disrupted its localization at 72 hours APF (Figures 6L–M). These data suggest that the subcellular localization of Side-IV and Side-VII are Beat-IIa/b and Beat-IV-dependent, respectively.

If Beat-IIa/b and Beat-IV defined the localization of Side-IV and Side-VII, they should also localize to the proximal area. We labeled the L4 morphology and analyzed the localization of Beat-IIb and Beat-IV with MiMIC-GFP transgenics.[38] We mainly focused on Beat-IV here, since Beat-IIb-MiMIC-GFP showed no localization on axons (Figures S8A–A", yellow arrowheads), but only in cell bodies (Figures S8A–A", yellow arrows), perhaps due to some defects in axonal transport. Beat-IV-MiMIC-GFP signal was seen only in the proximal area of L4 already at 72 hours APF (Figures S8B–B"). We then analyzed the co-localization of Side-VII and Beat-IV, and found Beat-IV localized to the proximal region before Side-VII (Figures S8C–D"). Futhermore, the localization

of Beat-IV is not dependent on Side-VII (Figures S8E–H'). These data suggest that Beat-IV localizes to the proximal region first, and then dictates Side-VII localization. In summary, Side-IV and Side-VII showed subcellular localization to the proximal region in a Beat-dependent manner.

Complex Formation of Side-IV with Kirre and Dysd-1 Restricts Loci of Synapse Formation and Inhibits Miswiring

The functional and localization analyses of Side-IV and Side-VII suggest that they instruct L2 to form synapses in the proximal region. The remaining question was why *side-IV* or *side-VII* mutants showed ectopic synapse formation in the distal region. A previous study reported that DIP-β causes L4 to prefer L2 as its synaptic partner over other neurons. The *dip-β* mutant resulted in miswiring to alternative neurons with ectopic synapse formation in the distal region.[3] Similarly, Side-IV and Side-VII may help L2 choose L4 as its synaptic partner and inhibit its miswiring to alternative neurons. In this case, there may be molecules that instruct miswiring of L2 to alternative neurons when *side-IV* or *side-VII* are absent.

Our analysis of *side-IV* in R7 suggested that Kirre can work as a co-receptor of Side-IV (Figure 3). Previous research reported that the *kirre* mutant resulted in total loss of postsynaptic structures of L4,[51] indicating that Kirre is a major presynaptic regulator in L2. Furthermore, single-cell-RNAseq data predicted unbiased interactions, homophilic self-interactions of Kirre and heterophilic Kirre-Rst interactions, between L2 and all other subtypes of lamina neurons.[13,16] We hypothesized that Kirre cooperates with Side-IV to establish L2-L4 connectivity but induces synaptic connection indiscriminately without Side-IV. In L2, Kirre showed the strongest localization in the proximal region, similar to

Side-IV (Figures 7A–B). However, Kirre localized more broadly than Side-IV, and some punctate signals were observed in the distal region (Figures 7A''', yellow arrowheads, B, and C). This indicates that Kirre localizes and interacts with Kirre/Rst not only in the proximal but also in the distal region. To assess whether Kirre is responsible for the ectopic synapse formation in the *side-IV* mutants, we tested genetic interactions between *kirre* mutant[52] and *side-IV* or *side-IV / side-VII* double mutants (Figures 7D–K). Deleting one copy of *kirre* decreased the number of synapses in the proximal region (Figures 7D–G and J–K), as well as suppressed ectopic synapse formation in the distal region (Figures 7E–I and K). These data indicate that Kirre promotes L2 miswiring with alternative neurons in the distal region in the *side-IV* or *side-IV* / *side-VII* double mutant.

The mechanism by which Side-IV can inhibit ectopic synapse formation in the distal region of the wild type is still elusive. One possibility is that some competitive mechanisms inhibit ectopic synapse formation. Since Side-IV and Side-VII localize specifically to the proximal region (Figure 6), they may compete with the molecules working in the distal region. A competitive synapse formation mechanism has been reported in R7.[5] While neurons extend several filopodia to search for synaptic partners, only one or two filopodia that recruit synapse seeding factors are stabilized at each time point.[5] Synaptic loci compete for the factors, since the amounts are limited and Dsyd-1 and Liprin-α are potential candidates for synapse seeding factors.[5] To test whether Dsyd-1 plays a role as a competing factor here, we knocked in a FLPase-based cell-specific GFP-tag to the Dsyd-1 locus and analyzed its endogenous localization (Figures 7L–T; see Methods). Dsyd-1 localized to the proximal region at 48 hours APF (Figures 7L–L''), and signals became punctate at 72 hours APF (Figures 7P and P'). *side-IV* or *side-IV / side-VII* double mutant flies showed leaky Dsyd-1 signals in the distal region at 48 hours APF

(Figures 7M–N''', yellow arrows, and O). Overall, the number of Dsyd-1 puncta decreased in the proximal region and increased in the distal region (Figures 7Q–T). These data indicate that Side-IV can anchor Dsyd-1 localization to the proximal region, not allowing the distally distributed molecules a chance to form synapses. Taken together, our results indicate that Side-IV may establish L2-L4 synapse specificity by cooperating with Kirre and Dsyd-1 in the proximal region, which can restrict synapse formation loci and inhibit miswiring.

DISCUSSION

This study identified Side-IV/Beat-IIb as a new key-lock combination that can induce synapse formation by establishing a cluster complex and signaling through its co-receptor Kirre or cytoplasmic signaling via Dsyd-1/Liprin-α in the *Drosophila* R7 photoreceptor. Side-IV regulates the loci of L2 synapse formation by anchoring Dsyd-1 to inhibit miswiring, with subcellular localization specified by Beat-IIa/b. We therefore propose a new key-lock complex formation model between the Beat and Side families for establishing synaptic specificity (Figure. 8).

Side-IV Establishes a Signaling Complex with Kirre and Dsyd-1

An essential observation is that Side-IV has the potential to induce synapse formation in the absence of its cytoplasmic domain (Figures 2E–E''', and J). Based on this observation, we hypothesized that Side-IV could induce signaling through co-receptors. We demonstrated that Side-IV and its co-receptor Kirre synergistically mediate signal transduction through the extracellular domain. Kirre is a well-known cell adhesion molecule and a member of the irre cell recognition module (IRM) family.[41] Its functions

range from nervous system-related processes such as axon guidance and synapse formation to myoblast aggregation and fusion, cell sorting, and other diverse biological phenomena.[41,51] *Cis*-regulation of Side-IV by such well-known cell adhesion molecules was surprising. Since co-expressing *side-IV* with other IRM members, *hbs* and *sns*, did not enhance the phenotype (data not shown), Kirre may function as a unique co-receptor for Side-IV. It is noted that there were some redundancies in the signaling of Side-IV/Kirre. The co-overexpression experiment in R7 showed that if either Side-IV or Kirre signaling pathway is active, meaning that the cytoplasmic domain of Side-IV or Kirre is present, the complex can induce a stronger phenotype (Figures 3G–P). This study indicates that Beat-Side family proteins may have unique co-receptors with cytoplasmic redundancy, and that their interplay could generate diverse connections.

Our study suggests that Dsyd-1 and Liprin-α work downstream of Side-IV. Side-IV strongly co-localized with Dsyd-1, but this co-localization significantly decreased when the PDZ-binding motif of Side-IV was deleted (Figures 4G–I). Furthermore, knockdown of *dsyd-1* specifically suppressed synaptic induction by cytoplasmic signaling of Side-IV (Figure 4M). Liprin-α co-localized with Side-IV through Dsyd-1, and knockdown of *liprin-a* strongly suppressed synaptic induction by Side-IV (Figures 4J–M). These data suggest that Dsyd-1 interacts with Side-IV's PDZ-binding motif and works with Liprin-α. In *Drosophila*, other synapse organization molecules Nrx-1 and Lar interact with Dysd-1 and Liprin-α, respectively.[44,53] Side-IV may compete with these molecules to recruit Dsyd-1 or Liprin-α.

Subcellular Localization of Side-IV and Side-VII Establishes L2-L4 Connectivity

Although Side-IV exhibits strong synapse induction abilities in R7, the *side-IV* mutant did not demonstrate any decrease in the number of synapses in lamina neurons (Figures 5C–D', and G). Such observation is quite common with other synapse organizers, such as Neurexins and Neuroligins; even knockdown or mutation of their three paralogues only slightly impacts synapse number despite their strong synapse-organizing abilities.[47,48] Conversely, notable ectopic synapse formation of *side-IV* in the distal region was observed (Figures 5C–D', and H).

Based on the expression data, three Beat-Side interactions are predicted between L2 and L4 (Figures 5A and B),[11,17] and the number of induced ectopic synapses in the distal region increased with disruption of these interactions. We confirmed that ectopic synapses were formed in L2 but not in other subtypes of lamina neurons (Figures 5I–L and S6). These findings indicate that several members of the Beat and Side families function redundantly to determine the loci of synapse formation in L2, specifically in the proximal region. This is supported by the localization analysis in which both Side-IV and Side-VII showed distinct subcellular localization to the proximal region in L2 which is defined by Beat-IIa/b and Beat-IV, respectively (Figures 6B–M). Despite uniform dendritic arborization of L2 from the proximal to distal areas,[49,50] the interplay between Beat-Side interactions and the non-uniform cellular morphology of L4 (dendrite distribution to the proximal region)[49] appears to establish non-uniform synapse formation restricted to the proximal region of L2. The DIP-β protein, which works at loci of L4 synapse formation, also showed substantial accumulation in the proximal region at 72 hours APF,[3] resembling the localization of Side-IV and Side-VII. The collaboration between DIP-Dpr and Beat-Side families is crucial in establishing L2-L4 connectivity.

Complex Formation of Side-IV Links Synaptic Specificity and Synaptogenesis

Synaptogenesis has a two-faced nature that is robust in establishing neural circuits, but can also be indiscriminate.[3,4,6,7] It is plausible that molecular coding, such as recognizing key-lock molecules, determines synaptic partners.[2,8] However, the loss of key-lock molecules sometimes results in miswiring with alternative partners.[3,4] Neurons can synapse with various partners, and key-lock molecules can bias synaptic partner preference. We initially sought to understand how preference for a synaptic partner is determined. Increasing the affinity between R7 and postsynaptic partners by homophilic interactions of CadE or hSDK2 alone did not induce synapse formation (Figure S3). Moreover, Side-IV $^{\Delta Cyto}$ couldn't completely rescue the ectopic synapse formation in *side-IV* (Figures S5A–D). These data indicate that some intracellular signaling mechanisms are required to increase preference and generate synaptic connection.[54]

Previous studies have demonstrated that DIP-β facilitates the preferential formation of synapses between L4 and L2 neurons specifically.[3] However, the exact intracellular signaling mechanisms remain elusive due to the absence of apparent intracellular signaling motifs in DIP-β.[16,55] The similarity in phenotypes between *dip-β* and *side-IV* mutants suggests that Side-IV also plays a role in facilitating L2 neurons' preference to form synapses with L4 neurons. Our study demonstrated that Dsyd-1 and Liprin-α, important signaling factors for active zone formation,[44,45] work downstream of Side-IV. Furthermore, Side-IV can anchor localization of Dsyd-1 to the proximal region, indicating that Side-IV causes accumulation of Dsyd-1 in L2-L4 contact sites and increases the L2 preference for L4. Simultaneously, competition for the synapse seeding factor Dsyd-1 is a limiting resource and can ensure relative preference for a synapse,[5,56] resulting in the inhibition of miswiring of L2. Similarly, Kirre, another major driver of

L2-L4 synaptogenesis,[51] can increase miswiring if not properly regulated (Figures 7D–K). These results suggest that establishing a signaling complex between key-lock molecules and synapse formation factors, with the appropriate ratio and subcellular localization, is crucial to achieving synaptic specificity. Our study proposes that one example of this is Side-IV complex formation with Kirre and Dsyd-1, which initiates synaptogenesis, coupled with the *trans*-synaptic interaction of Side-IV and Beat-IIb, which determines synaptic specificity.

ACKNOWLEDGMENT

We gratefully acknowledge Dr. Filipe Pinto-Teixeira at Molecular, Cellular and Developmental biology unit (MCD) in Center for Integrative Biology for providing the side-IV[MI10049]-T2AGal4 flies. We thank the Bloomington Drosophila Stock Center, Vienna Drosophila Resource Center (VDRC), Kyoto Drosophila Stock Center (Kyoto-Fly), and FlyORF for providing fly stocks. We thank Enago (www.enago.jp) for the English language review. This work was supported by JSPS KAKENHI #21J12660 (J. O.), a Grant-in-Aid for Scientific Research (B) and a Grant-in-Aid for Scientific Research on Innovative Areas from MEXT (#16H06457, #21H05682 and #21H02483 (T. S.)), a Takeda Visionary Research Grant from the Takeda Science Foundation (T. S.).

AUTHOR CONTRIBUTIONS

J.O., A.I., S.H.S., H.K., and T.S. designed experiments. J.O., A.I., S.H.S., and H.K., performed experiments and analyzed data. J.O., A.I., X.W., and R.I. generated transgenic reagents. J.O. and T.S. wrote the manuscript with reviewing from all co-authors.

DECLARATION OF INTERESTS

The authors declare that we have no competing interests.

REFERENCES

1. Sperry, R.W. (1963). CHEMOAFFINITY IN THE ORDERLY GROWTH OF NERVE FIBER PATTERNS AND CONNECTIONS. Proceedings of the National Academy of Sciences of the United States of America *50*, 703-710. 10.1073/pnas.50.4.703.
2. Sanes, J.R., and Zipursky, S.L. (2020). Synaptic Specificity, Recognition Molecules, and Assembly of Neural Circuits. Cell *181*, 536-556. 10.1016/j.cell.2020.04.008.
3. Xu, C., Theisen, E., Maloney, R., Peng, J., Santiago, I., Yapp, C., Werkhoven, Z., Rumbaut, E., Shum, B., Tarnogorska, D., et al. (2019). Control of Synaptic Specificity by Establishing a Relative Preference for Synaptic Partners. Neuron *103*, 865-877.e867. 10.1016/j.neuron.2019.06.006.
4. Kiral, F.R., Dutta, S.B., Linneweber, G.A., Hilgert, S., Poppa, C., Duch, C., von Kleist, M., Hassan, B.A., and Hiesinger, P.R. (2021). Brain connectivity inversely scales with developmental temperature in Drosophila. Cell Reports *37*, 110145. https://doi.org/10.1016/j.celrep.2021.110145.
5. Özel, M.N., Kulkarni, A., Hasan, A., Brummer, J., Moldenhauer, M., Daumann, I.M., Wolfenberg, H., Dercksen, V.J., Kiral, F.R., Weiser, M., et al. (2019). Serial Synapse Formation through Filopodial Competition for Synaptic Seeding Factors. Developmental cell *50*, 447-461.e448. 10.1016/j.devcel.2019.06.014.
6. Kiral, F.R., Linneweber, G.A., Mathejczyk, T., Georgiev, S.V., Wernet, M.F., Hassan, B.A., von Kleist, M., and Hiesinger, P.R. (2020). Autophagy-dependent filopodial kinetics restrict synaptic partner choice during Drosophila brain wiring. Nature communications *11*, 1325. 10.1038/s41467-020-14781-4.
7. Hiesinger, P.R. (2021). Brain wiring with composite instructions. BioEssays : news and reviews in molecular, cellular and developmental biology *43*, e2000166. 10.1002/bies.202000166.
8. Südhof, T.C. (2021). The cell biology of synapse formation. The Journal of cell biology *220*. 10.1083/jcb.202103052.
9. Takemura, S.Y., Bharioke, A., Lu, Z., Nern, A., Vitaladevuni, S., Rivlin, P.K., Katz, W.T., Olbris, D.J., Plaza, S.M., Winston, P., et al. (2013). A visual motion detection circuit suggested by Drosophila connectomics. Nature *500*, 175-181. 10.1038/nature12450.
10. Takemura, S.-y., Xu, C.S., Lu, Z., Rivlin, P.K., Parag, T., Olbris, D.J., Plaza, S., Zhao, T., Katz, W.T., Umayam, L., et al. (2015). Synaptic circuits and their variations within different columns in the visual system of Drosophila. Proceedings of the National Academy of Sciences of the United States of America *112*, 13711-13716. 10.1073/pnas.1509820112.

11. Davis, F.P., Nern, A., Picard, S., Reiser, M.B., Rubin, G.M., Eddy, S.R., and Henry, G.L. (2020). A genetic, genomic, and computational resource for exploring neural circuit function. eLife *9*, e50901. 10.7554/eLife.50901.
12. Cosmanescu, F., Katsamba, P.S., Sergeeva, A.P., Ahlsen, G., Patel, S.D., Brewer, J.J., Tan, L., Xu, S., Xiao, Q., Nagarkar-Jaiswal, S., et al. (2018). Neuron-Subtype-Specific Expression, Interaction Affinities, and Specificity Determinants of DIP/Dpr Cell Recognition Proteins. Neuron *100*, 1385-1400.e1386. 10.1016/j.neuron.2018.10.046.
13. Kurmangaliyev, Y.Z., Yoo, J., Valdes-Aleman, J., Sanfilippo, P., and Zipursky, S.L. (2020). Transcriptional Programs of Circuit Assembly in the Drosophila Visual System. Neuron *108*, 1045-1057.e1046. 10.1016/j.neuron.2020.10.006.
14. Özel, M.N., Simon, F., Jafari, S., Holguera, I., Chen, Y.C., Benhra, N., El-Danaf, R.N., Kapuralin, K., Malin, J.A., Konstantinides, N., and Desplan, C. (2021). Neuronal diversity and convergence in a visual system developmental atlas. Nature *589*, 88-95. 10.1038/s41586-020-2879-3.
15. Jain, S., Lin, Y., Kurmangaliyev, Y.Z., Valdes-Aleman, J., LoCascio, S.A., Mirshahidi, P., Parrington, B., and Zipursky, S.L. (2022). A global timing mechanism regulates cell-type-specific wiring programmes. Nature *603*, 112-118. 10.1038/s41586-022-04418-5.
16. Özkan, E., Carrillo, R.A., Eastman, C.L., Weiszmann, R., Waghray, D., Johnson, K.G., Zinn, K., Celniker, S.E., and Garcia, K.C. (2013). An extracellular interactome of immunoglobulin and LRR proteins reveals receptor-ligand networks. Cell *154*, 228-239. 10.1016/j.cell.2013.06.006.
17. Tan, L., Zhang, K.X., Pecot, M.Y., Nagarkar-Jaiswal, S., Lee, P.-T., Takemura, S.-Y., McEwen, J.M., Nern, A., Xu, S., Tadros, W., et al. (2015). Ig Superfamily Ligand and Receptor Pairs Expressed in Synaptic Partners in Drosophila. Cell *163*, 1756-1769. 10.1016/j.cell.2015.11.021.
18. Carrillo, R.A., Özkan, E., Menon, K.P., Nagarkar-Jaiswal, S., Lee, P.T., Jeon, M., Birnbaum, M.E., Bellen, H.J., Garcia, K.C., and Zinn, K. (2015). Control of Synaptic Connectivity by a Network of Drosophila IgSF Cell Surface Proteins. Cell *163*, 1770-1782. 10.1016/j.cell.2015.11.022.
19. Sergeeva, A.P., Katsamba, P.S., Cosmanescu, F., Brewer, J.J., Ahlsen, G., Mannepalli, S., Shapiro, L., and Honig, B. (2020). DIP/Dpr interactions and the evolutionary design of specificity in protein families. Nature communications *11*, 2125. 10.1038/s41467-020-15981-8.
20. Barish, S., Nuss, S., Strunilin, I., Bao, S., Mukherjee, S., Jones, C.D., and Volkan, P.C. (2018). Combinations of DIPs and Dprs control organization of olfactory receptor neuron terminals in Drosophila. PLoS genetics *14*, e1007560. 10.1371/journal.pgen.1007560.
21. suppXu, S., Xiao, Q., Cosmanescu, F., Sergeeva, A.P., Yoo, J., Lin, Y., Katsamba, P.S., Ahlsen, G., Kaufman, J., Linaval, N.T., et al. (2018). Interactions between the Ig-Superfamily Proteins DIP-α and Dpr6/10 Regulate Assembly of Neural Circuits. Neuron *100*, 1369-1384.e1366. 10.1016/j.neuron.2018.11.001.
22. Courgeon, M., and Desplan, C. (2019). Coordination between stochastic and deterministic specification in the Drosophila visual system. Science (New York, N.Y.) *366*. 10.1126/science.aay6727.

23. Venkatasubramanian, L., Guo, Z., Xu, S., Tan, L., Xiao, Q., Nagarkar-Jaiswal, S., and Mann, R.S. (2019). Stereotyped terminal axon branching of leg motor neurons mediated by IgSF proteins DIP-α and Dpr10. eLife *8*, e42692. 10.7554/eLife.42692.
24. Bornstein, B., Meltzer, H., Adler, R., Alyagor, I., Berkun, V., Cummings, G., Reh, F., Keren-Shaul, H., David, E., Riemensperger, T., and Schuldiner, O. (2021). Transneuronal Dpr12/DIP-δ interactions facilitate compartmentalized dopaminergic innervation of Drosophila mushroom body axons. The EMBO journal *40*, e105763. 10.15252/embj.2020105763.
25. Vactor, D.V., Sink, H., Fambrough, D., Tsoo, R., and Goodman, C.S. (1993). Genes that control neuromuscular specificity in Drosophila. Cell *73*, 1137-1153. 10.1016/0092-8674(93)90643-5.
26. Fambrough, D., and Goodman, C.S. (1996). The Drosophila beaten path gene encodes a novel secreted protein that regulates defasciculation at motor axon choice points. Cell *87*, 1049-1058. 10.1016/s0092-8674(00)81799-7.
27. Sink, H., Rehm, E.J., Richstone, L., Bulls, Y.M., and Goodman, C.S. (2001). sidestep encodes a target-derived attractant essential for motor axon guidance in Drosophila. Cell *105*, 57-67. 10.1016/s0092-8674(01)00296-3.
28. Siebert, M., Banovic, D., Goellner, B., and Aberle, H. (2009). Drosophila motor axons recognize and follow a Sidestep-labeled substrate pathway to reach their target fields. Genes Dev *23*, 1052-1062. 10.1101/gad.520509.
29. Li, H., Watson, A., Olechwier, A., Anaya, M., Sorooshyari, S.K., Harnett, D.P., Lee, H.-K.P., Vielmetter, J., Fares, M.A., Garcia, K.C., et al. (2017). Deconstruction of the beaten Path-Sidestep interaction network provides insights into neuromuscular system development. eLife *6*, e28111. 10.7554/eLife.28111.
30. Pipes, G.C., Lin, Q., Riley, S.E., and Goodman, C.S. (2001). The Beat generation: a multigene family encoding IgSF proteins related to the Beat axon guidance molecule in Drosophila. Development (Cambridge, England) *128*, 4545-4552. 10.1242/dev.128.22.4545.
31. Aberle, H. (2009). Searching for guidance cues: follow the Sidestep trail. Fly *3*, 270-273. 10.4161/fly.9790.
32. Zinn, K. (2009). Choosing the road less traveled by: a ligand-receptor system that controls target recognition by Drosophila motor axons. Genes & development *23*, 1042-1045. 10.1101/gad.1803009.
33. Kinold, J.C., Pfarr, C., and Aberle, H. (2018). Sidestep-induced neuromuscular miswiring causes severe locomotion defects in Drosophila larvae. Development (Cambridge, England) *145*. 10.1242/dev.163279.
34. Kind, E., Longden, K.D., Nern, A., Zhao, A., Sancer, G., Flynn, M.A., Laughland, C.W., Gezahegn, B., Ludwig, H.D.F., Thomson, A.G., et al. (2021). Synaptic targets of photoreceptors specialized to detect color and skylight polarization in Drosophila. eLife *10*, e71858. 10.7554/eLife.71858.
35. Heymann, C., Paul, C., Huang, N., Kinold, J.C., Dietrich, A.C., and Aberle, H. (2022). Molecular insights into the axon guidance molecules Sidestep and Beaten path. Frontiers in physiology *13*, 1057413. 10.3389/fphys.2022.1057413.
36. Karuppudurai, T., Lin, T.-Y., Ting, C.-Y., Pursley, R., Melnattur, Krishna V., Diao, F., White, Benjamin H., Macpherson, Lindsey J., Gallio, M., Pohida, T., and Lee, C.-H. (2014). A Hard-Wired Glutamatergic Circuit Pools and Relays

UV Signals to Mediate Spectral Preference in Drosophila. Neuron *81*, 603-615. https://doi.org/10.1016/j.neuron.2013.12.010.

37. Chen, Y., Akin, O., Nern, A., Tsui, C.Y., Pecot, M.Y., and Zipursky, S.L. (2014). Cell-type-specific labeling of synapses in vivo through synaptic tagging with recombination. Neuron *81*, 280-293. 10.1016/j.neuron.2013.12.021.

38. Nagarkar-Jaiswal, S., Lee, P.-T., Campbell, M.E., Chen, K., Anguiano-Zarate, S., Gutierrez, M.C., Busby, T., Lin, W.-W., He, Y., Schulze, K.L., et al. (2015). A library of MiMICs allows tagging of genes and reversible, spatial and temporal knockdown of proteins in Drosophila. eLife *4*, e05338. 10.7554/eLife.05338.

39. Tanaka, H., Miyazaki, N., Matoba, K., Nogi, T., Iwasaki, K., and Takagi, J. (2012). Higher-order architecture of cell adhesion mediated by polymorphic synaptic adhesion molecules neurexin and neuroligin. Cell reports *2*, 101-110. 10.1016/j.celrep.2012.06.009.

40. Gao, S., Takemura, S.Y., Ting, C.Y., Huang, S., Lu, Z., Luan, H., Rister, J., Thum, A.S., Yang, M., Hong, S.T., et al. (2008). The neural substrate of spectral preference in Drosophila. Neuron *60*, 328-342. 10.1016/j.neuron.2008.08.010.

41. Fischbach, K.F., Linneweber, G.A., Andlauer, T.F., Hertenstein, A., Bonengel, B., and Chaudhary, K. (2009). The irre cell recognition module (IRM) proteins. Journal of neurogenetics *23*, 48-67. 10.1080/01677060802471668.

42. Strutt, H., and Strutt, D. (2008). Differential stability of flamingo protein complexes underlies the establishment of planar polarity. Current biology : CB *18*, 1555-1564. 10.1016/j.cub.2008.08.063.

43. Hakeda-Suzuki, S., Berger-Müller, S., Tomasi, T., Usui, T., Horiuchi, S.Y., Uemura, T., and Suzuki, T. (2011). Golden Goal collaborates with Flamingo in conferring synaptic-layer specificity in the visual system. Nature neuroscience *14*, 314-323. 10.1038/nn.2756.

44. Owald, D., Khorramshahi, O., Gupta, V.K., Banovic, D., Depner, H., Fouquet, W., Wichmann, C., Mertel, S., Eimer, S., Reynolds, E., et al. (2012). Cooperation of Syd-1 with Neurexin synchronizes pre- with postsynaptic assembly. Nature neuroscience *15*, 1219-1226. 10.1038/nn.3183.

45. Fouquet, W., Owald, D., Wichmann, C., Mertel, S., Depner, H., Dyba, M., Hallermann, S., Kittel, R.J., Eimer, S., and Sigrist, S.J. (2009). Maturation of active zone assembly by Drosophila Bruchpilot. The Journal of cell biology *186*, 129-145. 10.1083/jcb.200812150.

46. Rivera-Alba, M., Vitaladevuni, S.N., Mishchenko, Y., Lu, Z., Takemura, S.Y., Scheffer, L., Meinertzhagen, I.A., Chklovskii, D.B., and de Polavieja, G.G. (2011). Wiring economy and volume exclusion determine neuronal placement in the Drosophila brain. Current biology : CB *21*, 2000-2005. 10.1016/j.cub.2011.10.022.

47. Varoqueaux, F., Aramuni, G., Rawson, R.L., Mohrmann, R., Missler, M., Gottmann, K., Zhang, W., Südhof, T.C., and Brose, N. (2006). Neuroligins determine synapse maturation and function. Neuron *51*, 741-754. 10.1016/j.neuron.2006.09.003.

48. Gokce, O., and Südhof, T.C. (2013). Membrane-tethered monomeric neurexin LNS-domain triggers synapse formation. The Journal of neuroscience : the

official journal of the Society for Neuroscience *33*, 14617-14628. 10.1523/jneurosci.1232-13.2013.

49. Fischbach, K.F., and Dittrich, A.P.M. (1989). The optic lobe of Drosophila melanogaster. I. A Golgi analysis of wild-type structure. Cell and Tissue Research *258*, 441-475. 10.1007/BF00218858.

50. Kolodziejczyk, A., Sun, X., Meinertzhagen, I.A., and Nässel, D.R. (2008). Glutamate, GABA and acetylcholine signaling components in the lamina of the Drosophila visual system. PLoS One *3*, e2110-e2110. 10.1371/journal.pone.0002110.

51. Lüthy, K., Ahrens, B., Rawal, S., Lu, Z., Tarnogorska, D., Meinertzhagen, I.A., and Fischbach, K.F. (2014). The irre cell recognition module (IRM) protein Kirre is required to form the reciprocal synaptic network of L4 neurons in the Drosophila lamina. Journal of neurogenetics *28*, 291-301. 10.3109/01677063.2014.883390.

52. Weavers, H., Prieto-Sánchez, S., Grawe, F., Garcia-López, A., Artero, R., Wilsch-Bräuninger, M., Ruiz-Gómez, M., Skaer, H., and Denholm, B. (2009). The insect nephrocyte is a podocyte-like cell with a filtration slit diaphragm. Nature *457*, 322-326. 10.1038/nature07526.

53. Kaufmann, N., DeProto, J., Ranjan, R., Wan, H., and Van Vactor, D. (2002). Drosophila liprin-alpha and the receptor phosphatase Dlar control synapse morphogenesis. Neuron *34*, 27-38. 10.1016/s0896-6273(02)00643-8.

54. Jiang, X., Sando, R., and Südhof, T.C. (2021). Multiple signaling pathways are essential for synapse formation induced by synaptic adhesion molecules. Proceedings of the National Academy of Sciences of the United States of America *118*. 10.1073/pnas.2000173118.

55. Lobb-Rabe, M., Nawrocka, W.I., Carrillo, R.A., and Özkan, E. (2023). Neuronal wiring receptors Dprs and DIPs are GPI anchored and this modification contributes to their cell surface organization. bioRxiv, 2023.2003.2002.530872. 10.1101/2023.03.02.530872.

56. Simon, F., and Konstantinides, N. (2021). Single-cell transcriptomics in the Drosophila visual system: Advances and perspectives on cell identity regulation, connectivity, and neuronal diversity evolution. Developmental biology *479*, 107-122. 10.1016/j.ydbio.2021.08.001.

57. Kondo, S., and Ueda, R. (2013). Highly improved gene targeting by germline-specific Cas9 expression in Drosophila. Genetics *195*, 715-721. 10.1534/genetics.113.156737.

58. Trush, O., Liu, C., Han, X., Nakai, Y., Takayama, R., Murakawa, H., Carrillo, J.A., Takechi, H., Hakeda-Suzuki, S., Suzuki, T., and Sato, M. (2019). N-Cadherin Orchestrates Self-Organization of Neurons within a Columnar Unit in the Drosophila Medulla. The Journal of Neuroscience *39*, 5861-5880. 10.1523/jneurosci.3107-18.2019.

59. Thorpe, H.M., and Smith, M.C. (1998). In vitro site-specific integration of bacteriophage DNA catalyzed by a recombinase of the resolvase/invertase family. Proceedings of the National Academy of Sciences of the United States of America *95*, 5505-5510. 10.1073/pnas.95.10.5505.

60. Hakeda-Suzuki, S., Takechi, H., Kawamura, H., and Suzuki, T. (2017). Two receptor tyrosine phosphatases dictate the depth of axonal stabilizing layer in the visual system. eLife *6*, e31812. 10.7554/eLife.31812.
61. Owald, D., Fouquet, W., Schmidt, M., Wichmann, C., Mertel, S., Depner, H., Christiansen, F., Zube, C., Quentin, C., Körner, J., et al. (2010). A Syd-1 homologue regulates pre- and postsynaptic maturation in Drosophila. Journal of Cell Biology *188*, 565-579. 10.1083/jcb.200908055.
62. Sugie, A., Hakeda-Suzuki, S., Suzuki, E., Silies, M., Shimozono, M., Möhl, C., Suzuki, T., and Tavosanis, G. (2015). Molecular Remodeling of the Presynaptic Active Zone of Drosophila Photoreceptors via Activity-Dependent Feedback. Neuron *86*, 711-725. 10.1016/j.neuron.2015.03.046.
63. Bolte, S., and Cordelières, F.P. (2006). A guided tour into subcellular colocalization analysis in light microscopy. Journal of microscopy *224*, 213-232. 10.1111/j.1365-2818.2006.01706.x.
64. Schindelin, J., Arganda-Carreras, I., Frise, E., Kaynig, V., Longair, M., Pietzsch, T., Preibisch, S., Rueden, C., Saalfeld, S., Schmid, B., et al. (2012). Fiji: an open-source platform for biological-image analysis. Nature methods *9*, 676-682. 10.1038/nmeth.2019.

LEGENDS TO FIGURES

Figure 1. The Interaction of Side-IV and Beat-IIb is Instructive for Synaptic Induction

(A−B") The synapse and axon of R7. Control (A−A"), *side-IV* OE (B−B"). Dotted lines indicate M1−M3 layer. Arrows and arrowheads indicate ectopic synapses and overshoot axons, respectively.

(C−E') Brp-GFP puncta of R7. *side-IV* OE in Wild Type (C and C'), *beat-IIa* mutant (D and D'), and *beat-IIb* mutant (E and E') background. Dotted lines indicate M1−M3 layer.

(F) Quantification of the number of the ectopic synapse (n > 60 axons).

(G) Quantification of the rate of overshoot axon (n >10 brains).

(H−H''') The localization of Beat-IIb and synapses of R7. Dotted lines indicate M1−M3 layer.

(I) The phenotypic scheme of *side-IV* OE.

(J−K'') The punctate signal of Beat-IIb by *side-IV* OE. Control (J−J''), *side-IV* OE (K−K''). Arrows indicate punctate Beat-IIb signal.

(L) Mutual localization of Side-IV, Beat-IIb, and Brp of R7. Dotted lines indicate M1−M3 layer. Arrows and arrowhead (L−L''') indicate co-localized Side-IV and Beat-IIb puncta with and without Brp-mCherry puncta, respectively.

(M) The summary scheme of Side-IV clusters, Beat-IIb clusters, and synaptic induction.

Statistical treatment of the number synapse and the rate of overshoot axon were analyzed with the Mann-Whitney test. In this and all following statistical significance. n.s. $P > 0.05$, * $P \leq 0.05$, ** $P \leq 0.01$, *** $P \leq 0.001$, **** $P \leq 0.0001$.

Figure 2. The Chimeric Analysis of Side-IV and mCD8

(A) The domain structure of Side-IV and mCD8.

(B) The variants of Side-IV domain deletion or chimera.

(C−G''') Mutual localization of Side-IV, Beat-IIb, and Brp of R7. Dotted lines indicate M1−M3 layer.

(H) Quantification of the rate of Side-IV-V5 variants clustered axon (n > 28 axons).

(I) Quantification of the rate of Beat-IIb clustered axon (n > 47 axons).

(J) Quantification of the number of the ectopic synapse (n > 32 axons).

(K) Quantification of the rate of overshot axon (n > 6 brains).

Statistical treatment of the rate of Side-IV-V5 variants or Beat-IIb clustered axon were analyzed with the Chi-square test. Statistical treatment of the number of the ectopic synapse and the rate of overshoot axon were analyzed with the Mann-Whitney test.

Figure 3. Kirre Interacts with Side-IV through the Extracellular Domain and Works as a Co-receptor

(A–E) The synapse and axon of R7. Control (A and A'), *kirre* OE (B and B'), Control UAS (*luciferase* RNAi) + *side-IV* OE (C and C'), *kirre* OE + *side-IV* OE (D and D'). Dotted lines indicate M1−M3 layer.

(E) Quantification of the number of the ectopic synapse (n > 44 axons).

(F) Quantification of the rate of overshoot axon (n > 4 brains).

(G−O) Photoreceptors in medulla with co-expression of *side-IV* and *kirre* variants. Control (G), *kirre* OE (H), *kirre* $^{\Delta Cyto}$ OE (I), *side-IV* OE (J), *side-IV* + *kirre* OE (K), *side-IV*+*kirre* $^{\Delta Cyto}$ OE (L), *side-IV* $^{\Delta Cyto}$ OE (M), *side-IV* $^{\Delta Cyto}$ + *kirre* OE (N), *side-IV* $^{\Delta Cyto}$ + *kirre* $^{\Delta Cyto}$ OE (O).

(P) Quantification of the rate of overshoot axon (n > 4 brains).

(Q−V) Protein accumulation at cell boundaries in transiently transfected S2 cells subjected to aggregation assay. The S2 cells were co-transfected with Act5c-gal4. UAS-*side-IV*-mCherry and UAS-*kirre*-GFP (Q–Q"). (R) Distribution of accumulation ratio of Side-IV and Kirre. UAS-*side-IV*-mCherry and UAS-*cadE*-GFP (S–S"). (T) Distribution of accumulation ratio of Side-IV and CadE. (U) Distribution of accumulation ratio of Side-IV co-transfected with Kirre, Kirre $^{\Delta Cyto}$, or CadE. (V) Distribution of

accumulation ratio of Side-IV variants co-transfected with Kirre. The sample size is indicated (n).

Statistical treatment of the number of synapse and the rate of overshoot axon were analyzed with the Mann-Whitney test. Distribution of the cell-cell contact accumulation ration was analyzed with the unpaired t-test.

Figure 4. Side-IV Transduces a Signal with Dsyd-1 and Liprin-α through the Cytoplasmic Tail

(A−D) The synapse and axon of R7.Control (A and A', same images as 3A and A'), Control RNAi (*luciferase* RNAi) + *side-IV* OE (B and B', same images as 3C and C'), *dsyd-1* RNAi + *side-IV* OE (C and C'), *liprin-α* RNAi + *side-IV* OE (D and D'). Dotted lines indicate M1−M3 layer.

(E) Quantification of the number of the ectopic synapse (n > 69 axons).

(F) Quantification of the rate of overshoot axon (n > 6 brains).

(G−H") The localization of Side-IV and Dsyd-1. The S2 cells were co-transfected with Act5c-gal4, UAS-*dsyd-1*-mCherry, and UAS-*side-IV*^{FL}-GFP or UAS-*side-IV*$^{\Delta PDZb}$. Side-IV^{FL}-GFP and Dsyd-1-mCherry (G−G"), Side-IV$^{\Delta PDZb}$-GFP and Dsyd-1-mCherry (H−H").

(I) The quantification of the co-localization (n > 35 images).

(J−K") The localization of Side-IV and Liprin-α. The S2 cells were co-transfected with UAS-*side-IV*-GFP, UAS-*liprin-a*-mCherry with and without UAS-*dsyd-1*-V5. Side-IV-

GFP and Liprin-α-mCherry (J−J''), Side-IV-GFP, Liprin-α-mCherry, and Dsyd-1-V5 (K−K'').

(L) The quantification of the co-localization (n > 35 images).

(M) Quantification of the number of ectopic synapses (n > 43 axons) represented as mean ± SD.

(N) The working model of synaptic induction by Side-IV.

Statistical treatment of the number of synapse and the rate of overshoot axons were analyzed with the Mann-Whitney test. Statistical treatment of the Co-localization index was analyzed with the unpaired t-test.

Figure 5. *side-IV* and *side-VII* are Required for Proper Synapse Formation Patterns of the L2 Neurons

(A) Scheme of synaptic connection patterns of lamina neurons in lamina.

(B) Scheme of predicted Beat-Side interactions between L2 and L4 neurons.

(C−F') The presynaptic structures and cell morphology of Lamina neuron (LN). Control (C and C'), *side-IV*$^{\Delta 4\text{-}1}$ mutant (D and D'), *side-VII*$^{\Delta E3\text{-}4\text{-}1}$ mutant (E and E'), *side-IV* / *side-VII* double mutant (F and F'). Dotted lines indicate the proximal and distal boundary.

(G) Quantification of the number of synapses in the proximal region (n > 82 axons).

(H) Quantification of the number of synapses in the distal region (n > 107 axons).

(I−J') The synapse and axon of L2. Control (I and I'), *side-IV*$^{\Delta 4\text{-}1}$ / *side-VII*$^{\Delta E3\text{-}4\text{-}1}$ double mutant (J and J'). Dotted lines indicate the proximal and distal boundary.

(K) Quantification of synapses in the proximal region of the L2 neuron (n > 88 axons).

(L) Quantification of synapses in the distal region of the L2 neuron (n > 84 axons). Statistical treatment of the number of synapses in the proximal region and distal region were analyzed with the unpaired t-test and Mann-Whitney test, respectively.

Figure 6. Side-IV and Side-VII Showed Beats-dependent Subcellular Localization in the Proximal Region

(A−A''') Mutual localization of endogenous Brp, Side-IV, and Side-VII at 72h after pupal formation (APF). Merge (A), Brp (A'), Side-IV (A''), and Side-VII (A'''). Dotted lines indicate the proximal and distal boundary.

(B−C') Localization of Side-IV (B and B') and Side-VII (C and C') in the L2 neuron. Dotted lines indicate the boundary between the proximal and distal region.

(D−G') Endogenous localization of Side-IV in the lamina neuron. Control 48h APF (D and D'), *beat-IIa*$^{+2}$ mutant + *beat-IIb* RNAi 48h APF (E and E'). Control 72h APF (F and F'), *beat-IIa*$^{+2}$ mutant + *beat-IIb* RNAi 72h APF (G and G'). Dotted lines indicate the proximal and distal boundary.

(H) Quantification of the rate of the axons with Side-IV localization in the proximal region in the 72h APF (n > 149 axons).

(I−M') Endogenous localization of Side-VII in the lamina neuron. Control 48h APF (I and I'), *beat-IV* RNAi 48h APF (J and J'). Control 72h APF (L and L'), *beat-IV* RNAi 72h APF (M and M'). Dotted lines indicate the proximal and distal boundary.

(H) Quantification of the rate of the axons with Side-VII localization in the proximal region in the 72h APF (n > 147 axons).

Statistical treatment of the rate of Side-IV or Side-VII positive axon was analyzed with the Chi-square test.

Figure. 7 Side-IV Limit the Dysd-1 Localization in the Proximal and Inhibit the Synapse Formation by Kirre in the Distal Region.

(A) The mutual localization Kirre and Side-IV on L2 neuron at 72h APF. Merge (A), magnified Merge (A'), Side-IV-GFP (A''), Kirre-HA (A'''). Compared with Side-IV localization, Kirre puncta signals were observed in the distal region (yellow arrowheads in A'''). Dotted lines indicate the proximal and distal boundary.

(B) The fluorescent intensity of Side-IV-GFP (green) and Kirre-HA (magenta) measured from proximal to distal across L2 axons as shown in A'' and A''' (dotted lines). The average intensity of 29 axons was calculated.

(C) Schematic of Side-IV (green) and Kirre (magenta) localization in the L2 neuron.

(D−I) The presynaptic structures of lamina neurons. Control (D, same image as 5C'), *side-IV* mutant (E), *side-IV* / *side-VII* double mutant (F, same image as 5F'), *kirre* heterozygous mutant (G), *kirre* heterozygous and *side-IV* mutant (H), *kirre* heterozygous and *side-IV* / *side-VII* double mutant. Dotted lines indicate the proximal and distal boundary.

(H) Quantification of synapses in the proximal region (n > 69 axons).

(H) Quantification of synapses in the distal region (n > 79 axons).

(L−N'') The localization of endogenous Dsyd-1 in lamina neurons at 48h APF. Control (L−L''), *side-IV* mutant (M−M''), *side-IV* / *side-VII* double mutant (N−N''). Dotted lines indicate the proximal and distal boundary.

(O) The rate of Dsyd-1 diffused axon in the distal region (n > 92 axons).

(P−R') The localization of Dsyd-1 in lamina neuron at 72h APF Control (P and P'), *side-IV* mutant (Q and Q'), *side-IV* / *side-VII* double mutant (R and R'). Dotted lines indicate the proximal and distal boundary.

(S) Quantification of the number of Dsyd-1 puncta in the proximal region (n > 120 axons).

(T) Quantification of the number of Dsyd-1 puncta in the distal region (n > 96 axons).

Statistical treatment of the number of Brp-GFP or Dsyd-1 puncta in the proximal region and distal region were analyzed with the unpaired t-test and Mann-Whitney test, respectively. The rate of Dsyd-1 diffused axon was analyzed with by the Chi-square test.

Figure. 8 Side-IV-Beat-IIb's Complex Formation Model.

The new key-lock combination Side-IV-Beat-IIb made cluster complex and transduced bifurcated signaling through co-receptor, Kirre and scaffold protein complex, Dsyd-1-Liprin-α. Side-IV can specific the loci of synapse formation and anchor the Dsyd-1 to inhibit miswiring.

LEGENDS TO SUPPLEMENTAL FIGURES

Figure S1. Mis-expression of *side-IV* in R7 induced ectopic synapse formation in the M1–M3 layer. (A and B) The Beat/Side double knockdown experiments. Quantification of the number of synapses in the M1−M3 layer (A) and M4−6 layer (B) per axon. Control

(n=119 axons/4 brains), *beat-IIb* & *beat-IIIc* RNAi (n=70/4), *side* & *side-III* RNAi (n=164/6), *side* & *side-V* RNAi (n=184/7), *side* & *side-VII* RNAi (n=108/4), *side-III* & *side-V* RNAi (n=118/4), *side-III* & *side-VII* RNAi (n=96/4), *side-V* & *side-VII* (n=100/4). (C and D) The Beat/Side overexpression (OE) experiments. Quantification of the number of synapses in the M1−M3 layer (C) and M4−6 layer (D) per axon. Control (n=119 axons/4 brains), *beat-IIa* OE (n=145/6), *beat-IIb* OE (n=145/6), *beat-VI* OE (n=71/4), *side* OE (n=132/4), *side-IV* OE (n=40/2), *side-VII* OE (n=34/2), *side-VIII* OE (n=104/4). (E) Scheme of tissue-specific visualization of endogenous Side-IV. The FRT-stop-FRT-GFP cassette was knocked in just before the stop codon of *side-IV*. By expressing FLPase, endogenous localization of Side-IV can be observed in a tissue-specific manner. (F and F') Localization of Side-IV in the optic lobe at the adult stage. heatshock-FLP was used to visualize Side-IV in all cells. (G–I') Expression of endogenous *side-IV* of R7 in a developmental stage. The endogenous Side-IV on R7 was visualized with *side-IV*-FsF-GFP and 20C11-FLP. Axons of photoreceptor R7 were visualized with U-myr-RFP (magenta, GMR-FsF-Gal4 with 20C11-FLP). 24 h APF (G–G'), 48 h APF (H–H'), 72 h APF (I–I'). No Side-IV-GFP signals were observed at any stages, indicating that R7 doesn't endogenously express *side-IV*. Statistical treatment of the number of Brp-GFP puncta in the M1−M3 layer and M4−M6 layer were analyzed with the Mann-Whitney test and unpaired t-test, respectively. In this and all following statistical treatment; n.s. $P > 0.05$, * $P \leq 0.05$, ** $P \leq 0.01$, *** $P \leq 0.001$, **** $P \leq 0.0001$.

910 **Figure S2. The Domain deletion analysis of *side-IV* in R7 and S2 cultural cells.** (A)
911 Domain structure of Side-IV. (B−H') The Brp-GFP signal of R7 with overexpression (OE)
912 of *side-IV* domain deletion variants. The Brp-GFP puncta (green) in R7 is visualized by
913 combining the STaR method with 20C11-FLP. Photoreceptors were visualized by 24B10
914 (magenta). Control (B and B'), *side-IV* ^{FL} OE (C and C'), *side-IV* $^{\Delta Ig1\text{-}5}$ OE (D and D'),
915 *side-IV* $^{\Delta Ig1}$ OE (E and E'), *side-IV* $^{\Delta FnIII}$ OE (F and F'), *side-IV* $^{\Delta Cyto}$ OE (G and G'), *side-*
916 *IV* $^{\Delta PDZb}$ OE (H and H'). Orange dotted lines indicate region of M1−M3 layer. (I)
917 Quantification of the number of synapses in the M1−M3 layer per axon. Control (n= 84
918 axons/5 brains), *side-IV* ^{FL} OE (n= 60/5), *side-IV* $^{\Delta Ig1\text{-}5}$ OE (n= 57/5), *side-IV* $^{\Delta Ig1}$ OE (n=
919 70/5), *side-IV* $^{\Delta FnIII}$ OE (n= 86/7), *side-IV* $^{\Delta Cyto}$ OE (n= 33/3), *side-IV* $^{\Delta PDZ}$ OE (n= 45/4).
920 (J) Quantification of the rate of overshoot axon per optic lobe. Control (n=12 brains),
921 *side-IV* ^{FL} OE (n= 10), *side-IV* $^{\Delta Ig1\text{-}5}$ OE (n= 12), *side-IV* $^{\Delta Ig1}$ OE (n= 10), *side-IV* $^{\Delta FnIII}$ OE
922 (n= 10), *side-IV* $^{\Delta Cyto}$ OE (n=13), *side-IV* $^{\Delta PDZ}$ OE (n= 12). (K) Quantification of the rate
923 of Beat-IIb clustered per axon. Control (n= 81 axons/4 brains), *side-IV* ^{FL} OE (n= 161/7),
924 *side-IV* $^{\Delta Ig1\text{-}5}$ OE (n= 91/4), *side-IV* $^{\Delta Ig1}$ OE (n= 133/6), *side-IV* $^{\Delta FnIII}$ OE (n= 82/4), *side-IV*
925 $^{\Delta Cyto}$ OE (n= 68/4), *side-IV* $^{\Delta PDZ}$ OE (n= 80/4). (L−P") Cell aggregation assay with
926 *Drosophila* S2 cell. S2 cells were individually transfected with UAS-*side-IV* variants or
927 *mcd8*-mCherry or UAS-*beat-IIb*-GFP. All cells were co-transfected with Actin5C-gal4.
928 After the transfection, cells were mixed together. Side-IV ^{FL}-mCherry vs Beat-IIb-GFP
929 (L−L"), Side-IV $^{\Delta Ig1}$-mCherry vs Beat-IIb-GFP (M−M"), Side-IV $^{\Delta Ig1-5}$-mCherry vs Beat-
930 IIb-GFP (N−N"), mCd8-mCherry vs Beat-IIb-GFP (O−O"), and Side-IV $^{Ecto\Delta FnIII}$::mCD8

931 vs Beat-IIb-GFP (P−P''). Yellow dotted blankets represent cell aggregations. (Q) The
932 quantification of the number of cells per cell aggregation. Side-IV ^{FL}-mCherry vs Beat-
933 IIb-GFP (n=70 cell aggregations), Side-IV $^{\Delta Ig1}$-mCherry vs Beat-IIb-GFP (n=51), Side-
934 IV $^{\Delta Ig1-5}$-mCherry vs Beat-IIb-GFP (n=40), mCd8-mCherry vs Beat-IIb-GFP (n=48),
935 Side-IV $^{Ecto\Delta FnIII}$::mCD8 vs Beat-IIb-GFP (n=86). Statistical treatment of the number of
936 synapses in the M1−M3 layer, the rate of overshoot axons, and the number of cell per cell
937 aggregation were analyzed with the Mann-Whitney test. Statistical treatment of the rate
938 of Beat-IIb clustered axon was performed with the Chi-square test.
939
940 **Figure S3. Synapse was induced in the M1−M3 layer in R7 by introducing Nrxs-Nlgs**
941 **interactions but not CadE or hSDK2 homophilic interactions.** (A−E') The Brp-GFP
942 signal of R7 with overexpression (OE) of *nrx-1* or *nlg1−3* with FlySAM in both R7 and
943 postsynaptic neuron by combining GMR-gal4 and Ort-gal4. The Brp-GFP puncta (green)
944 in R7 is visualized by combining the STaR method with 20C11-FLP. Photoreceptors were
945 visualized by 24B10 (magenta) Control (A and A'), *nrx-1* OE (B and B'), *nlg-1* OE (C and
946 C'), *nlg-2* OE (D and D'), *nlg-3* OE (E and E'). (F) Quantification of the number of
947 synapses in the M1-M3 layer per axon. Control (n= 114 axons/5 brains), *nrx-1* OE (n=
948 157 /5), *nlg-1* OE (n= 169/5), *nlg-2* OE (n= 58/3), *nlg-3* OE (n= 114/4). (G−I) The Brp-
949 GFP signal of R7 by overexpressing the molecules which have homophilic interaction in
950 R7 and postsynaptic neuron by combining GMR-gal4 and Ort-gal4. Control (G and G'),

951 *cadE* OE (H and H'), *hsdk2* OE (I and I'). Orange dotted lines indicate region of M1−M3

952 layer. (I) Quantification of the number of synapses in the M1−M3 layer per axon. Control

953 (n= 109 axons/7 brains), *cadE* OE (n= 67/5), *hSDK2* OE (n=73/5). Statistical treatment

954 of the number of synapses in the M1−M3 layer was analyzed with the Mann-Whitney test.

955

956 **Figure S4. The biochemical and genetic interaction between Side-IV and Kirre.**

957 (A) The result of Co-IP for Side-IV and Kirre. S2 cell were transfected with Actin5C-gal4

958 and UAS-*side-IV*-V5/GFP and/or UAS-*kirre*-GFP/V5. Immunoprecipitation (IP) and

959 Immunoblotting (blot) were performed with α-GFP and α-V5, respectively. The bands

960 between 100 kDa and 150 kDA were detected only when cells expressed both *side-IV* and

961 *kirre*, showing they make complex with interaction. Predicted molecular weights of Side-

962 IV and Kirre are about 110 kDa and 101kDa, respectively. (B) Aggregation assay of S2

963 cell transfected Actin5C-gal4 and UAS-*mcd8*-mCherry against Actin5C-gal4 and UAS-

964 *kirre*-GFP. Homophilic interaction of Kirre causes Kirre-transfected S2 cells to form

965 aggregates (Kirre-GFP cluster). (C) Aggregation assay of S2 cell transfected Actin5C-

966 gal4 and UAS-*side-IV*-mCherry against Actin5C-gal4 and UAS-*kirre*-GFP. (D)

967 Quantification of the rate of Kirre-GFP cluster that contains mCherry positive cell. If

968 Side-IV interacts with Kirre in *trans*, many of Kirre-GFP clusters should contain *side-IV*-

969 mCherry expressing cells. There was no significance of the rate of Kirre-GFP cluster that

970 has mCherry positive cell between aggregation assay of mCd8-mCherry vs Kirre-GFP

971 and Side-IV-mCherry vs Kirre-GFP, indicating Side-IV didn't interact with Kirre in *trans*.

972 The sample size is indicated (n). Statistical treatment was performed with the Chi-square

973 test. (E–L) Photoreceptors in medulla with co-expression of *side-IV* variant *kirre* with

974 GMR-gal4. *side-IV* $^{\Delta Ig1-5}$ OE (E), *side-IV* $^{\Delta Ig1-5}$ + *kirre* OE (F), *side-IV* $^{\Delta Ig1}$ OE (G), *side-*

975 *IV* $^{\Delta Ig1}$ + *kirre* OE (H), *side-IV* $^{\Delta FnIII}$ OE (I), *side-IV* $^{\Delta FnIII}$ + *kirre* OE (J), *side-IV* $^{\Delta PDZb}$ OE

976 (K), *side-IV* $^{\Delta PDZb}$ + *kirre* OE (L). (M) Quantification of the rate of overshoot axon with

977 *side-IV* variants and *kirre*. Control (n=12 brains), *kirre* OE (n=4), *side-IV* ^{FL} OE (n=10),

978 *side-IV* ^{FL} + *kirre* OE (n=6), *side-IV* $^{\Delta Ig1-5}$ OE (n=12), *side-IV* $^{\Delta Ig1-5}$ + *kirre* OE (n=6), *side-*

979 *IV* $^{\Delta Ig1}$ OE (n=10), *side-IV* $^{\Delta Ig1}$ + *kirre* OE (n=6), *side-IV* $^{\Delta FnIII}$ OE (n=10), *side-IV* $^{\Delta FnIII}$ OE

980 + *kirre* OE (n=7), *side-IV* $^{\Delta Cyto}$ OE (n=13), *side-IV* $^{\Delta Cyto}$ + *kirre* OE (n=6), *side-IV* $^{\Delta PDZb}$

981 OE (n=12), *side-IV* $^{\Delta PDZb}$ + *kirre* OE (n=5). Statistical treatment of the rate of the Kirre-

982 GFP cell cluster with mCherry positive cell and the rate of overshoot axon was performed

983 with the Chi-square test and the Mann-Whitney test, respectively.

984

985 **Figure S5. Disruption of Side-IV-Beat-IIa/b or Side-VII-Beat-IV interactions results**

986 **in ectopic synapse formation in the distal region.** (A–C') Brp-GFP of lamina neuron in

987 rescue experiment. *side-IV*$^{\Delta 4-1/T2A-gal4}$ (A and A'), *side-IV*$^{\Delta 4-1/T2A-gal4}$ + Side-IV ^{FL} (B and

988 B'), *side-IV*$^{\Delta 4-1/T2A-gal4}$ + Side-IV $^{\Delta Cyto}$ (C and C'). Orange dotted lines indicate the

989 boundary between the proximal and distal region. (D) Quantification of Brp-GFP puncta

990 in the distal region in the rescue experiment. *side-IV*$^{\Delta 4-1/+}$ (n= 88 axons/ 3 brains), *side-IV*

991 $^{T2A-gal4/+}$ (n= 90/3), *side-IV* $^{\Delta 4-1/T2A-gal4}$ (n= 134/4), *side-IV*$^{\Delta 4-1/T2A-gal4}$ + Side-IV ^{FL} (n= 90/3),

992 *side-IV*$^{\Delta 4-1/T2A-gal4}$ + Side-IV $^{\Delta Cyto}$ (n= 86/3). (E–G') Brp-GFP of lamina neuron in L2

993 specific *side-IV* or *side-VII* mutant. L2 neuron (magenta, L2) were visualized by

994 combining UAS-myr-RFP with L2-specific gal4 driver (GMR16H03-gal4). L2-specific

995 *side-IV* or *side-VII* mutant means *side-IV*$^{\Delta 4\text{-}1}$ or *side-VII*$^{\Delta E3\text{-}4\text{-}1}$ heterozygote with L2-
996 specific RNAi [GMR16H03-Gal4, UAS-RNAi]). Control (E and E'), L2 specific *side-IV*
997 mutant (F and F'), L2 specific *side-VII* mutant (G and G'). Orange dotted lines indicate
998 the boundary between the proximal and distal region. (H) Quantification of Brp-GFP
999 puncta in L2 specific *side-IV* or *side-VII* mutant. Control (n=96 axons/3 brains), L2
1000 specific *side-IV* mutant (n=160/4), L2 specific *side-VII* mutant (n=129/3). (I–L') Brp-GFP
1001 of lamina neuron in *beat* mutants. Control (I and I'), *beat-IIa*$^{+2}$ mutant (J and J'), *beat-*
1002 *IIb*$^{\Delta 14}$ mutant (K and K'), *beat-IV*$^{\Delta 65}$ mutant (L and L'). Brp-GFP puncta (green) of all
1003 lamina neurons are visualized by combining the STaR method and R27G05-FLP. And
1004 Lamina neuron (LN) is visualized with LexAop-myrtdTOM (magenta). Orange dotted
1005 lines indicate the boundary between the proximal and distal region. (M–N') Brp-GFP of
1006 lamina neurons when *beat-IIb* were knocked down on *beat-IIa* mutant background.
1007 Control (M and M'), *beat-IIa*$^{+2}$ mutant + *beat-IIb* RNAi (J and J'). *beat-IIb* was knocked
1008 down specifically in lamina neurons (Ay-gal4 & R27G05-FLP) and lamina neurons were
1009 visualized with UAS-myr-RFP (magenta). Orange dotted lines indicate the boundary
1010 between the proximal and distal region. (O) Quantification of Brp-GFP puncta in the
1011 distal region in *beat* single mutants. Control (n=161 axons/3 brains), *beat-IIa*$^{+2}$ mutant
1012 (n=191/3), *beat-IIb*$^{\Delta 14}$ mutant (n=102/3), *beat-IV*$^{\Delta 65}$ mutant (n=133/3). (P) Quantification
1013 of Brp-GFP puncta in the distal region of lamina neurons upon simultaneous loss of *beat-*
1014 *IIa* and *beat-IIb*. Control (n=144 axons/3 brains), *beat-IIa*$^{+2}$ mutant + *beat-IIb* RNAi
1015 (n=129/3). Statistical processing of the number of Brp-GFP puncta in the distal region of
1016 the lamina neuron was analyzed with the Mann-Whitney test.
1017

1018 **Figure S6. *side-IV* and *side-VII* double mutants didn't form ectopic synapses in the**
1019 **Distal region of L1, L3, L4, and L5 neurons.** (A–H') Brp-GFP (green) and axons
1020 (magenta) of lamina neurons with different sub-type. (A–B') L1 neuron. Control (A and
1021 A'), *side-IV*$^{\Delta 2}$ / *side-VII*$^{\Delta E3\text{-}4\text{-}1}$ double mutant (B and B') expressing FLPase specifically in
1022 the L1 neuron (R48A08-AD (II), R66A01-DBD (III) L1 split-GAL4 + UAS-FLP). (C–
1023 D') L3 neuron. Control (C and C'), *side-IV*$^{\Delta 2}$ / *side-VII*$^{\Delta E3\text{-}4\text{-}1}$ double mutant (D and D')
1024 expressing FLPase specifically in L3 neuron (R64B03-AD (II), R14B07-DBD (III) L3
1025 split-GAL4 + UAS-FLP). (E–F') L4 neuron. Control (E and E'), *side-IV*$^{\Delta 2}$ / *side-VII*$^{\Delta E3\text{-}4\text{-}1}$
1026 double mutant (F and F') expressing FLPase specifically in L4 neuron (R31C06-AD (II),
1027 R34G07-DBD (III) L4 split-GAL4 + UAS-FLP). Orange dotted lines indicate the
1028 boundary between the proximal and distal region. (G–H') L5 neuron. Control (G and G'),
1029 *side-IV*$^{\Delta 2}$ / *side-VII*$^{\Delta E3\text{-}4\text{-}1}$ double mutant (H and H') expressing FLPase specifically in L5
1030 neuron (R64D07-AD (II), R37E10-DBD (III) L5 split-GAL4 + UAS-FLP). (I)
1031 Quantification of Brp-GFP puncta in the proximal region of the L4 neuron. Control
1032 (n=124 axons/3 brains), *side-IV*$^{\Delta 2}$ / *side-VII*$^{\Delta E3\text{-}4\text{-}1}$ double mutant (n=123/3). (J)
1033 Quantification of Brp-GFP puncta in the distal region of the L4 neuron. Control (n=191
1034 axons/3 brains), *side-IV*$^{\Delta 2}$ / *side-VII*$^{\Delta E3\text{-}4\text{-}1}$ double mutant (n=191/3). Statistical treatment
1035 of the number of Brp-GFP puncta in the proximal region and distal region of the L4
1036 neuron were analyzed with the unpaired t-test and Mann-Whitney test, respectively.
1037
1038 **Figure S7. L2 neurons express *side-IV* and *side-VII* from developmental to adult.** (A–

1039 H') Endogenous expression of *side-IV* or *side-VII* in L2 neuron. Side-IV and Side-VII
1040 were visualized by combining UAS-FLP with L2-gal4 (R16H03-gal4) or L2-split-gal4
1041 (R53G02-AD (II), R29G11-DBD (III)) against *side-IV*-FsF-GFP or *side-VII*-FsF-GFP.
1042 *side-IV* expression in L2 neuron at 24h APF (A and A'), 48h APF (B and B'), 72h APF (C
1043 and C'), 0d after eclosion (D and D'). Orange dotted lines indicate the boundary between
1044 the proximal and distal region. *side-VII* expression in L2 neuron at 24h APF (E and E'),
1045 48h APF (F and F'), 72h APF (G and G'), 0d after eclosion (H and H'). Orange dotted
1046 lines indicate the boundary between the proximal and distal region.
1047

1048 **Figure S8. Localization Beat-IIb and Beat-IV in the lamina neuron.** (A−A")
1049 Localization of Beat-IIb in the lamina neuron at the 72 hours APF. Localization of Beat-
1050 IIb was visualized by *beat-IIb*-MiMIC-GFP (green). The morphology of the L4 neuron
1051 was visualized with the L4 neuron-specific gal4 driver (GMR31C06-gal4) against UAS-
1052 myr-RFP (magenta). No Beat-IIb-GFP signal was observed in the axon of the L4 neuron
1053 (yellow arrowheads), although the Beat-IIb-GFP signal was confirmed in the cell body of
1054 the L4 neuron (yellow arrows). It suggests that *beat-IIb*-MiMIC-GFP is expressed in the
1055 L4 neuron, however, it may not be transported correctly to the axon. (B−B") Localization
1056 of Beat-IV in the lamina neurons at the 72 hours APF. Localization of Beat-IV was
1057 visualized by *beat-IV*-MiMIC-GFP (green). A strong Beat-IV-GFP signal was observed
1058 on the axon in the proximal region of the L4 neuron. (C−D") Analysis of the mutual
1059 localization of Side-VII and Beat-IV. Side-VII was visualized by combining *side-VII*-
1060 FsF-mCherry (magenta) and R27G05FLP. Beat-IV was visualized by *beat-IV*-MiMIC-

GFP (green). Orange dotted lines indicate the boundary between the proximal and distal region. At the 60h APF (C−C''). Side-VII localized from proximal to distal (C'') while Beat-IV showed a subcellular localization in the proximal region (C''). At the 66h APF (D−D''). Side-VII is strongly localized in the proximal region (D'') with strong colocalization with Beat-IV (D''). (E−H') Analysis of the Beat-IV localization dependency to Side-VII in the lamina neurons. Control 48h APF (E and E'), *side-VII* RNAi 48h APF (F and F'), Control 72h APF (G and G'), *side-VII* RNAi 72h APF (H and H'). *side-VII* was knocked down in lamina neurons (Ay-gal4 & R27G05-FLP). Beat-IV similarly localized in the proximal region, indicating the localization of Beat-IV is not Side-VII dependent.

SUPPLEMENTALY TABLE

Table S1, The list of genotypes of flies used in this study.

Table S2, The list of oligonucleotides used in this study.

Table S3, The list of mutant alleles generated in this study.

RESOURCE AVAILABILITY

Lead Contact

Further information and requests for resources and reagents should be directed to and will be fulfilled by the Lead Contact, Takashi Suzuki (suzukit@bio.titech.ac.jp).

Material Availability

All unique reagents generated in this study are available from the Lead Contact without restriction.

METHODS

Key Resource Table

REAGENT or RESOURCE	SOURCE	IDENTIFIER
Antibodies		
mouse anti 24B10	DSHB	Cat#24B10, RRID: AB_528161
rat anti cadN	DSHB	Cat#DN-Ex#8, RRID:AB_528121
mouse V5 Tag Monoclonal Antibody	ThermoFisher	Cat#R960-25, RRID:AB_2556564
Anti-HA High Affinity; Rat monoclonal antibody (clone 3F10)	Roche	Cat#11867423001, RRID:AB_390918
Anti-Myc Tag Antibody, clone 4A6	Millipore	Cat# 05-724MG, RRID:AB_568800
rabbit GFP Polyclonal Antibody	ThermoFisher	Cat#A-11122, RRID:AB_221569
Alexa Fluor 488 Goat anti-Mouse	ThermoFisher	Cat#A11029, RRID:AB_2534088
Alexa Fluor 568 Goat anti-Mouse	ThermoFisher	Cat#11031, RRID:AB_144696
Alexa Fluor 633 Goat anti-Mouse	ThermoFisher	Cat#A-21052, RRID:AB_2535719
Alexa Fluor 488 Goat anti-Rat	ThermoFisher	Cat#A-11006, RRID:AB_141373
Alexa Fluor 568 Goat anti-Rat	ThermoFisher	Cat#A-11077, RRID:AB_141874
Goat anti-Mouse IgG (H+L) Secondary Antibody, HRP	ThermoFisher	Cat#32430, RRID:AB_1185566
Biological Samples		
RE17794 (cDNA for *beat-IIa*)	Drosophila Genomics Resource Center	RRID:DGRC_8501
RE17755 (cDNA for *beat-IIb*)	Drosophila Genomics Resource Center	RRID:DGRC_1090247
GH14967 (cDNA for *side-VII*)	Drosophila Genomics Resource Center	RRID:DGRC_4843
Critical Commercial Assays		
KOD One® PCR Master Mix	TOYOBO	Cat#KMM-101
NEBuilder® HiFi DNA Assembly Master Mix	BioLabs	Cat#E2621X
FastGene Plasmid Mini Kit	NIPPON Genetics	Cat#FG-90502
FastGene Gel/PCR Extraction Kit	NIPPON Genetics	Cat#FG-91302
Pierce™ Protein A Magnetic Beads	ThermoFisher	Cat#88845
7.5% Mini-PROTEAN® TGX™ Precast Protein Gels	BIO-RAD	Cat#4561025
Trans-Blot Turbo Mini 0.2 µm PVDF Transfer Packs	BIO-RAD	Cat#1704156

Experimental Models: Organisms/Strains		
GMR-gal4	Bloomington Drosophila Stock Center	BDSC_8605, RRID:BDSC_8605
GMR-FsF-gal4	Chen et al., 2014	N/A
ort-gal4 (X)	Gao et al., 2008	N/A
ort-gal4 (III)	Bloomington Drosophila Stock Center	BDSC_56519, RRID:BDSC_56519
Ay-gal4	Bloomington Drosophila Stock Center	BDSC_4413, RRID:BDSC_4413
R48A08-p65.AD (L1-AD)	Bloomington Drosophila Stock Center	BDSC_70707, RRID:BDSC_70707
R66A01-GAL4.DBD (L1-DBD)	Bloomington Drosophila Stock Center	BDSC_68999, RRID:BDSC_68999
R48A08-p65.AD (L2-AD)	Bloomington Drosophila Stock Center	BDSC_70707, RRID:BDSC_70707
R66A01-GAL4.DBD (L2-DBD)	Bloomington Drosophila Stock Center	BDSC_68999, RRID:BDSC_68999
GMR16H03-Gal4 (L2-gal4)	Bloomington Drosophila Stock Center	BDSC_48744, RRID:BDSC_48744
R64B03-p65.AD (L3-AD)	Bloomington Drosophila Stock Center	BDSC_75895, RRID:BDSC_75895
R14B07-GAL4.DBD (L3-DBD)	Bloomington Drosophila Stock Center	BDSC_68940, RRID:BDSC_68940
R31C06-p65.AD (L4-AD)	Bloomington Drosophila Stock Center	BDSC_70646, RRID:BDSC_70646
R34G07-GAL4.DBD (L4-DBD)	Bloomington Drosophila Stock Center	BDSC_69029, RRID:BDSC_69029
GMR31C06-gal4 (L4-gal4)	Bloomington Drosophila Stock Center	BDSC_49883, RRID:BDSC_49883
R64B07-p65.AD (L5-AD)	Bloomington Drosophila Stock Center	BDSC_71106, RRID:BDSC_71106
R37E10-GAL4.DBD (L5-DBD)	Bloomington Drosophila Stock Center	BDSC_69000, RRID:BDSC_69000
side-IV[MI10049]-T2AGal4	Gift From Filipe Pinto-Teixeira	N/A
kirre^{sps}	Weavers et al., 2009	N/A
P{SAM.dCas9.GS05146}attP40 (Nrx-1)	Bloomington Drosophila Stock Center	BDSC_82741, RRID:BDSC_82741
P{SAM.dCas9.GS04053}attP40 (Nlg-1)	Bloomington Drosophila Stock Center	BDSC_81419, RRID:BDSC_81419
P{SAM.dCas9.GS04054}attP40 (Nlg-2)	Bloomington Drosophila Stock Center	BDSC_81420, RRID:BDSC_81420
P{SAM.dCas9.GS05201}attP40 (Nlg-3)	Bloomington Drosophila Stock Center	BDSC_82936, RRID:BDSC_82936
UAS-FLP (X)	Bloomington Drosophila Stock Center	BDSC_8208, RRID:BDSC_8208
UAS-FLP (II)	Bloomington Drosophila Stock Center	BDSC_4539, RRID:BDSC_4539
UAS-myr-RFP (III)	Bloomington Drosophila Stock Center	BDSC_7119, RRID:BDSC_7119
UAS-myr-RFP (II)	Bloomington Drosophila Stock Center	BDSC_7118, RRID:BDSC_7118
UAS-*luciferase*-RNAi (Control RNAi)	Bloomington Drosophila Stock Center	BDSC_35788, RRID:BDSC_35788

UAS-*beat-IIb*-RNAi	Vienna Drosophila Resource Center	VDRC_104935, RRID:FlyBase_FBst0479711
UAS-*beat-IIIc*-RNAi	Vienna Drosophila Resource Center	VDRC_27137, RRID:FlyBase_FBst0456776
UAS-*beat-IV*-RNAi	Vienna Drosophila Resource Center	VDRC_110257, RRID:FlyBase_FBst0481835
UAS-*side*-RNAi	Vienna Drosophila Resource Center	VDRC_1283, RRID:FlyBase_FBst0450699
UAS-*side-III*-RNAi (II)	Vienna Drosophila Resource Center	VDRC_101967, RRID:FlyBase_FBst0482037
UAS-*side-III*-RNAi (III)	Vienna Drosophila Resource Center	VDRC_22742, RRID:FlyBase_FBst0454672
UAS-*side-IV*-RNAi	Vienna Drosophila Resource Center	VDRC_16636, RRID:FlyBase_FBst0452368
UAS-*side-V*-RNAi (II)	Vienna Drosophila Resource Center	VDRC_44997, RRID:FlyBase_FBst0465867
UAS-*side-V*-RNAi (III)	Vienna Drosophila Resource Center	VDRC_44997, RRID:FlyBase_FBst0465867
UAS-*side-VII*-RNAi (II)	Vienna Drosophila Resource Center	VDRC_106353, RRID:FlyBase_FBst0472832
UAS-*side-VII*-RNAi (III)	Vienna Drosophila Resource Center	VDRC_106353, RRID:FlyBase_FBst0472832
UAS-*kirre*-RNAi	Vienna Drosophila Resource Center	VDRC_27227, RRID:FlyBase_FBst0456824
UAS-*dsyd-1*-RNAi	Bloomington Drosophila Stock Center	BDSC_32946, RRID:BDSC_32946
UAS-*liprin-α*-RNAi	Bloomington Drosophila Stock Center	BDSC_53868, RRID:BDSC_53868
P{EP}*side-VIII*	Bloomington Drosophila Stock Center	BDSC_17248, RRID:BDSC_17248
UAS-*beat-VI-HA*	FlyORF	RRID:FlyBase_FBst0502390
UAS-*shg (cadE)*	Bloomington Drosophila Stock Center	BDSC_58494, RRID:BDSC_58494
UAS-*hSDK2-HA*	Bloomington Drosophila Stock Center	BDSC_78487, RRID:BDSC_78487
UAS-*kirre-HA*	Bloomington Drosophila Stock Center	BDSC_92196, RRID:BDSC_92196
UAS-myc-*liprin-α*	Bloomington Drosophila Stock Center	BDSC_63809, RRID:BDSC_63809
UAS-*dsyd-1*	Owald et al., 2010	N/A
brp-FsF-GFP (III)	Bloomington Drosophila Stock Center	BDSC_55753, RRID:BDSC_55753
brp-FsF-V5-LexA, LexAop-tdTomato	Bloomington Drosophila Stock Center	BDSC_56142, RRID:BDSC_56142
20C11-FLPG5	Bloomington Drosophila Stock Center	BDSC_55766, RRID:BDSC_55766
R27G05-FLPG5	Bloomington Drosophila Stock Center	BDSC_55765, RRID:BDSC_55765
hs-FLP	Bloomington Drosophila Stock Center	BDSC_5258, RRID:BDSC_5258
Mi{PT-GFSTF.0}beat-IIb[MI03102-GFSTF.0]	Bloomington Drosophila Stock Center	BDSC_59406, RRID:BDSC_59406
Mi{PT-GFSTF.1}beat-IV[MI05715-GFSTF.1]	Bloomington Drosophila Stock Center	BDSC_66506, RRID:BDSC_66506

nos-Cas9 (attp40)	Bloomington Drosophila Stock Center	BDSC_78781, RRID:BDSC_78781
nos-Cas9 (attp2)	Bloomington Drosophila Stock Center	BDSC_78782, RRID:BDSC_78782
vas-int.Dm(ZH-2A); PBac{y[+]-attP-3B}(VK00037)	Bloomington Drosophila Stock Center	BDSC_24872, RRID:BDSC_24872
vas-int.Dm(ZH-2A); PBac{y[+]-attP-3B}(VK00033)	Bloomington Drosophila Stock Center	BDSC_24871, RRID:BDSC_24871
P{y[+t7.7] v[+t1.8]=TKO.GS04527}attP40 (TRiP-KO for *side-IV*)	Bloomington Drosophila Stock Center	BDSC_82064, RRID:BDSC_82064
P{y[+t7.7] v[+t1.8]=WKO.5-C1}attP40 (TRiP-KO for *beat-IV*)	Bloomington Drosophila Stock Center	BDSC_84159, RRID:BDSC_84159
beat-IIa^{+2}	This paper	N/A
beat-IIb$^{\Delta 14}$	This paper	N/A
beat-IV$^{\Delta 65}$	This paper	N/A
side-IV$^{\Delta 4\text{-}1}$	This paper	N/A
side-IV$^{\Delta 4\text{-}2}$	This paper	N/A
side-VII$^{\Delta E3\text{-}4\text{-}1}$	This paper	N/A
side-VII$^{\Delta E3\text{-}4\text{-}2}$	This paper	N/A
side-VII$^{\Delta E3\text{-}4\text{-}1}$, *side-IV*$^{\Delta 2}$	This paper	N/A
UAS-*beat-IIa*	This paper	N/A
UAS-*beat-IIb*	This paper	N/A
UAS-*side*	This paper	N/A
UAS-*side-IV*	This paper	N/A
UAS-*side-IV-V5*	This paper	N/A
UAS-*side-IV*-GFP	This paper	N/A
UAS-*side-IV* $^{\Delta Ig1\text{-}5}$	This paper	N/A
UAS-*side-IV* $^{\Delta Ig1}$	This paper	N/A
UAS-*side-IV* $^{\Delta FnIII}$	This paper	N/A
UAS-*side-IV* $^{\Delta Cyto}$ *-V5*	This paper	N/A
UAS-*side-IV* $^{\Delta PDZb}$	This paper	N/A
UAS-*side-IV*$^{Ecto\Delta FnIII}$*::mCD8-V5*	This paper	N/A
UAS-*side-IV*^{Ecto}*::mCD8*$^{TM+Cyto}$*-V5*	This paper	N/A
UAS-*side-VII*	This paper	N/A
UAS-*side-VII*-GFP	This paper	N/A
UAS-*kirre* $^{\Delta Cyto}$*-HA*	This paper	N/A
brp-FsF-GFP (II)	This paper	N/A
brp-FsF-mCherry (II)	This paper	N/A
side-IV-FsF-GFP	This paper	N/A
side-VII-FsF-GFP	This paper	N/A
side-VII-FsF-mCherry	This paper	N/A
dsyd-1-FsF-GFP	This paper	N/A
Oligonucleotides		
Please refer to Table S1.	This paper	N/A
Software and Algorithms		
Imaris 8.2.0	Bitplane	http://www.bitplane.com/imaris
NIS-elements VERSION 4.11	Nikon	https://www.nis-elements.cz/en
Prism	Graphpad	https://www.graphpad.com/ scientific-software/prism/

Fiji	Schindelin et al., 2012	https://fiji.sc/
Other		
All of the genotypes used in this paper are listed in Table S2.	This paper	N/A

Generation of transgenic flies

side-IV-FsF-GFP, *side-VII*-FsF-GFP (mCherry), *brp*-FsF-GFP (mCherry), and *dsyd-1*-FsF-GFP knock-in allele were generated by CRISPR/Cas9 technology.[57] A knock-in vector containing the homology arms, the flip-out cassette with GFP (FRT-stop-FRT-GFP (mCherry), were generated as described previously.[58] The oligo DNAs used for amplification of *side-IV*, *side-VII*, *brp*, and *dsyd-1* fragments and creating gDNA are listed in Table S1. A gRNA vectors were created and cloned into pBFv-U6.2 vector and were injected to eggs of nos-Cas9 (attp40) or nos-Cas9 (attp2) flies at WellGenetics or Bestgene together with the knock-in vector. The precise integration of the knock-in vector was verified by PCR and sequencing.

Mutant alleles of *beat-IIa*, *beat-IIb*, *beat-IV*, *side-IV*, and *side-VII* were generated by CRISPR/Cas9 technology.[57] The gRNA vectors were created and cloned into pBFv-U6.2 vector for *beat-IIa*, *beat-IIb*, and *side-VII*. TRiP-KO lines (BDSC 84159, BDSC 82064) were used to generate mutant alleles of *beat-IV* and *side-IV*. For generating *side-IV* / *side-VII* double mutant, we introduced frameshift mutation *side-IV*$^{\Delta 2}$ on *side-VII*$^{\Delta E3\text{-}4\text{-}1}$ allele by using TRiP-KO line (BDSC 82064). The oligo DNAs used for generating mutant alleles and all the mutations of mutant alleles are shown in Table S1 and Table S3, respectively.

UAS lines were generated φC31 integrase-mediated recombination.[59] The cDNAs were cloned into pUAST-attB vector and injected to egg of vas-int.Dm(ZH-2A);

PBac{y[+]-attP-3B}(VK00037) or vas-int.Dm(ZH-2A); PBac{y[+]-attP-3B}(VK00033) at Wellgenetics. The full length of cDNAs were amplified from cDNA clones (RE17794 for *beat-IIa*, RE17755 for *beat-IIb*, ECD01053 for *side-IV*, GH14967 for *side-VII*). The available cDNA clones of *beat-IIb* (RE17755) and *side-IV* (ECD01053) didn't cover all of the coding sequences. We amplified the lacking sequences from the fly genome and conjected the full length of cDNAs. We conjected 2 fragments (F1 & F2) by overlap pcr for generating insertions of Side-IV domain deletion variants, Side-IV-mCD8 chimeras, and GFP tagged Side-IV or Side-VII. To generate the V5 or GFP tagged Side-IV and Side-VII constructs, GS-linker were inserted before the V5 or GFP. Furthermore, the sequence of PDZ binding motif of Side-IV or Side-VII were inserted in after the V5 or GFP not to disrupt the function of PDZ binding motif. The primers used to generate the UAS lines are shown in Table S1.

Immunohistochemistry and imaging

The flies were maintained under standard conditions in Drosophila media at a temperature of 25˚C. As described previously, the experimental procedures for brain dissection, fixation, and immunostaining were performed as described previously.[60] Fly brains were dissected in 0.1% PBT (PBS containing Triton X-100) and then fixed with 4% paraformaldehyde at room temperature for 60 min. A primary antibody was added and incubated overnight at 4 degrees on a shaker. The next day, the samples were washed with 0.1 % PBT 3 times and incubated at room temperature for 60 min. The secondary antibody was added and incubated at room temperature for 60 min. Samples were washed with 0.1% PBT 3 times and incubated at room temperature for 2 hr. Finally, samples were washed with PBS once and replaced by VECTASHIELD®. The following antibodies

were used for immunohistochemistry: mAb24B10 (1:50, DSHB), rat antibody to CadN (Ex#8, 1:50, DSHB), mouse antibody to V5 (R960, 1:400, Invitrogen), rat antibody to HA (3F10, 1:50, Roche). To enhance the signal intensity of Beat-IIb-MiMIC-GFP and Beat-IV-MiMIC-GFP, rabbit antibody to GFP conjugated with Alexa488 (1:400, Life technologies) was used. The secondary antibodies were Alexa488-, Alexa568- or Alexa633-conjugated (1:400, Life Technologies). For image acquisition S2 cells, they were fixed 4% paraformaldehyde at room temperature for 30 min and washed with PBS for 30min.

Image acquisition

All confocal images were taken by Nikon C2+ or A1 confocal microscope with NIS elements (version 4.11). Each brain image was acquired between the depths of 30 and 50 μm from the surface of brain with a Z step size of 0.5 or 1μm. Images were acquired twice and averaged. Images were processed with NIS elements (Nikon), Adobe Photoshop, and Adobe illustrator.

Cell culture transfection and Co-immunoprecipitation

We used a mixture of culture medium; 500mL of Schneider's Drosophila Medium (×1, gibco), 5mL of Penicillin-Streptomycin Solution (×100, wako), and 50mL of fetal bovine serum (Sigma). S2 cells were grown in 24 well plates (TrueLine) with 500 μL of the culture medium. For transfection, 1.5mg of UAS vectors and pActin5C-Gal4 were co-transfected and incubated with 10mL of HilyMax (DOJINDO) and 30mL of Schneider's Drosophila Medium. For co-immunoprecipitation, 3 wells of S2 cells were lysed in Lysis Buffer (50 mM Tris at pH 6.8, 150 mM NaCl, 1% NP40, protease inhibitor cocktail

[Roche]), immunoprecipitated with 1 μg of GFP antibody (Life Technologies) and Protein A beads (Pierce) according to the manufacture's procedure. SDS-PAGE was performed on 7.5% SDS-PAGE gels (Bio-Rad). Immunoblotting was performed by V5 antibody (R960, 1:2500, Invitrogen) and HRP secondary antibody (REF32430, 1:1000, Invitrogen). The images were taken by ImageQuant LAS 4000mini (cytiva) with Chemiluminescent HRP Substrate (MILLIPORE).

pUAS plasmids were generated by cloning cDNAs into pUAST-GFP or mCherry vectors. To amplify cDNA or domain deletion variants of *side-IV*, we used the same primers as generate transgenic flies. Genome extractions were performed to amplify the cDNA of *kirre* (UAS-*kirre.C-HA*, BDSC 92196), *cadE* (UASp-*shg.R*, BDSC58494), *dsyd-1* (UAS-*dsyd-1*),[61] and *liprin-a* (UAS-MYC-*liprin-a.H*, BDSC63809). All of primers used to generate the pUAS plasmids are shown in Table S1.

QUANTIFICATION AND STATISTICAL ANALYSIS

All of the names of samples were randomized before the quantification. The number of Brp puncta of lamina neurons and photoreceptor R7 was counted manually with IMARIS (version 8.2.0) as described previously.[62] The Brp puncta on a 3D image were identified with the spot function of IMARIS (diameter was set to 0.35μm). For the separation of the region of proximal region and distal region of lamina neurons, we cropped each stack of the proximal and distal ROI with NIS elements and a pen tablet (Cintiq 13HD, Wacom). We first drew the lines on the top and bottom of the lamina cartridge. Next, we drew a line on the midpoint of the lamina cartridge referring to the top and bottom lines. The accept region function of NIS-elements was then used to select the regions above and below the midpoint lines, which were then cropped as the proximal and distal regions,

respectively. The number of Dsyd-1 puncta in the proximal region and distal region at 72h APF were counted as the same method. The rate of overshoot axon was calculated manually with NIS elements, by counting the number of photoreceptors that overshoot beyond M6 layer and dividing the total number of axons.

In Figure 1M, the Side-IV cluster with Beat-IIb cluster was calculated manually with IMARIS, by counting the number of Side-IV puncta that co-localized with Beat-IIb puncta and dividing the total number of Side-IV puncta in the M1–M3 layer. The Side-IV & Beat-IIb cluster with Brp was calculated, by counting the number of Side-IV puncta co-localized with Beat-IIb and Brp puncta and dividing the total number of Side-IV puncta co-localized with Beat-IIb puncta.

In Figures 2H, I, and S2K the rate of Side-IV or Beat-IIb clustered axon were calculated manually with IMARIS, by the counting the number of axons with Side-IV or Beat-IIb clustered signal in the M1–M3 layer and dividing the total number of axons.

In Figures 3R, T, and U–V, the cell-cell contact accumulation ratio was calculated manually with NIS-elements as described previously.[43] Calculate the average intensity of GFP or mCherry signal on cell-cell border by drawing the line ROI and dividing the average intensity on the membrane, which did not contact other cells.

In Figures 4I and L, Pearson's Coefficient was calculated with the JACoP plugin on Fiji.[63,64]

In Figures 6H and M, the rate of Side-IV or Side-VII positive axon was calculated manually with NIS elements, by counting the number of the axon that has Side-IV or Side-VII signal to the proximal region and dividing the total number of axons.

In Figure 7B, the average intensity along the Proximal to Distal regions of Side-IV and Kirre in the L2 neuron was calculated by drawing a linear ROI using NIS-elements and calculating the average intensity.

In Figure 7O, the rate of Dsyd-1 positive axon (Distal) was calculated manually with NIS-elements, by counting the number of the axon that has Dsyd-1 signal on the distal region and dividing the total number of the axon at 48h APF.

In Figure S2Q, the number of cells per cell aggregation was calculated manually with NIS-elements, by counting the total number of cells on each cell aggregation. The cell cluster with contains both GFP and mCherry expressing cells was identified as cell aggregation.

In Figure S4D, the rate of Kirre-GFP cell cluster with and without mCherry positive cell was calculated manually with NIS-elelments, by counting the rate of Kirre-GFP cell cluster which had more than one mCherry positive cell. The cell cluster with more than two GFP expressing cells was identified as Kirre-GFP cell cluster.

Statistical analysis

All of the statistical analysis are described in the figure legends. Statistical significance. n.s. $P > 0.05$, * $P \leq 0.05$, ** $P \leq 0.01$, *** $P \leq 0.001$, **** $P \leq 0.0001$.

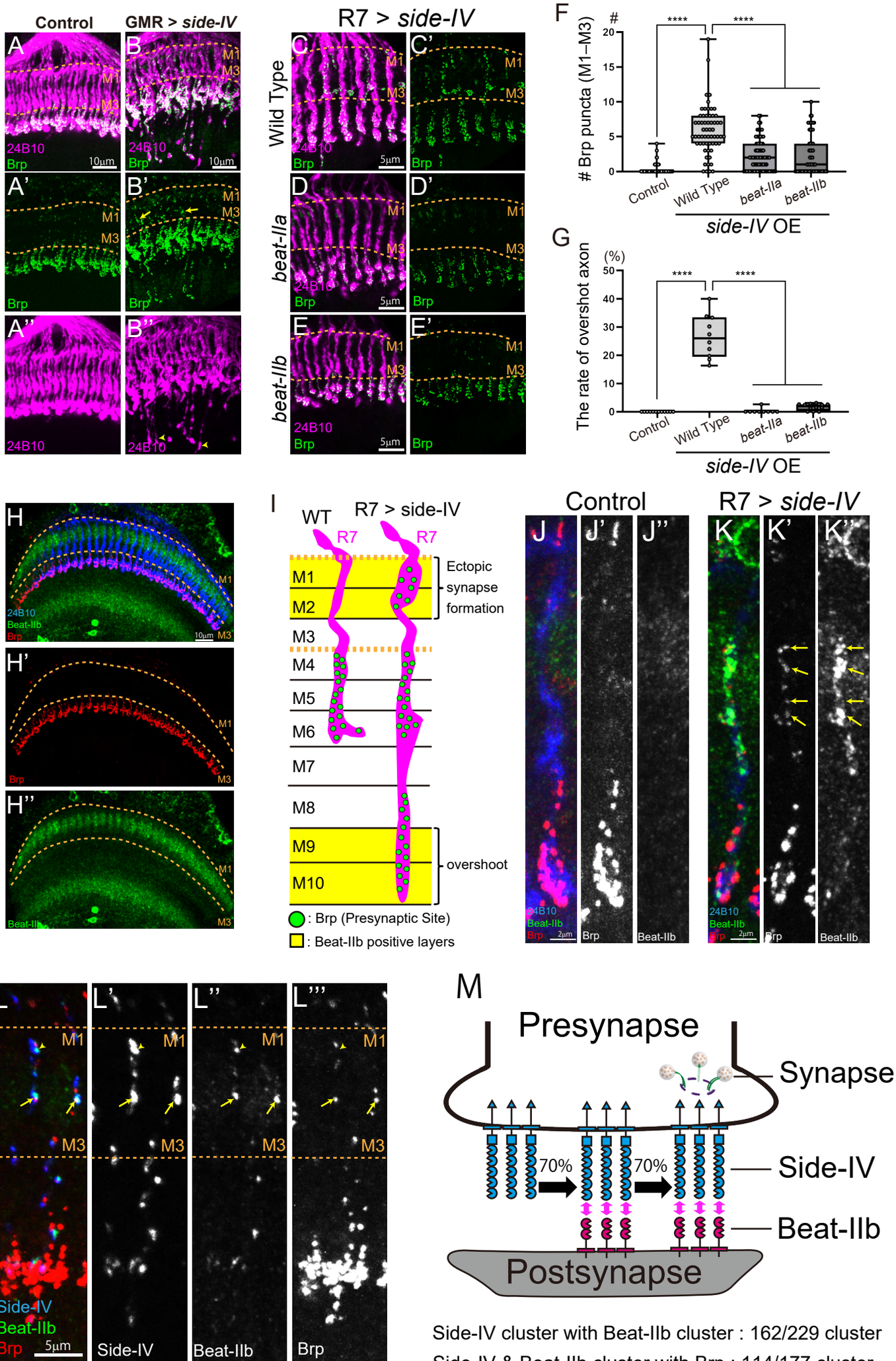
Control
GMR > side-IV
R7 > side-IV
Wild Type
beat-IIa
beat-IIb
M1
M3
24B10
Brp
10μm
5μm
F
Brp puncta (M1–M3)
Control
Wild Type
beat-IIa
beat-IIb
side-IV OE
G
The rate of overshot axon
(%)
H
H'
H''
Beat-IIb
I
WT
R7 > side-IV
R7
Ectopic synapse formation
M1
M2
M3
M4
M5
M6
M7
M8
M9
M10
overshoot
: Brp (Presynaptic Site)
: Beat-IIb positive layers
Control
R7 > side-IV
J
J'
J''
K
K'
K''
2μm
L
L'
L''
L'''
Side-IV
Beat-IIb
Brp
M
Presynapse
Synapse
70%
70%
Side-IV
Beat-IIb
Postsynapse
Side-IV cluster with Beat-IIb cluster : 162/229 cluster
Side-IV & Beat-IIb cluster with Brp : 114/177 cluster

Figure 1

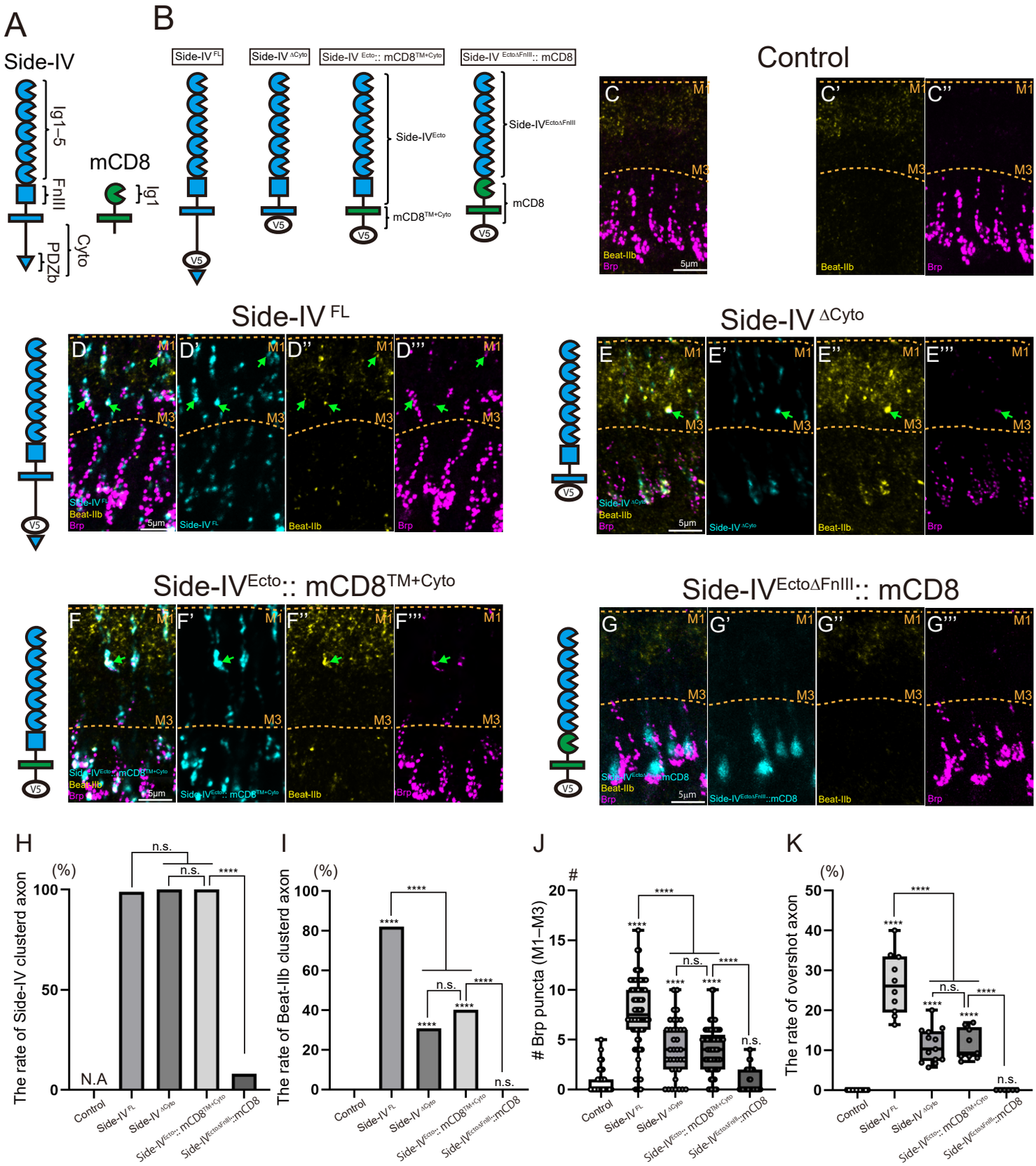
A
Side-IV
Ig1–5
FnIII
Cyto
PDZb
mCD8
Ig1
B
Side-IV FL
Side-IV ΔCyto
Side-IV Ecto:: mCD8TM+Cyto
Side-IV EctoΔFnIII:: mCD8
Side-IVEcto
mCD8TM+Cyto
Side-IVEctoΔFnIII
mCD8
V5
Control
C
C'
C''
M1
M3
Beat-IIb
Brp
5μm
Side-IV FL
D
D'
D''
D'''
Side-IV ΔCyto
E
E'
E''
E'''
Side-IVEcto:: mCD8TM+Cyto
F
F'
F''
F'''
Side-IVEctoΔFnIII:: mCD8
G
G'
G''
G'''
H
The rate of Side-IV clusterd axon
(%)
n.s.
****
N.A
Control
Side-IV FL
Side-IV ΔCyto
Side-IVEcto:: mCD8TM+Cyto
Side-IVEctoΔFnIII::mCD8
I
The rate of Beat-IIb clusterd axon
(%)
J
Brp puncta (M1–M3)
#
K
The rate of overshot axon
(%)

Figure 2

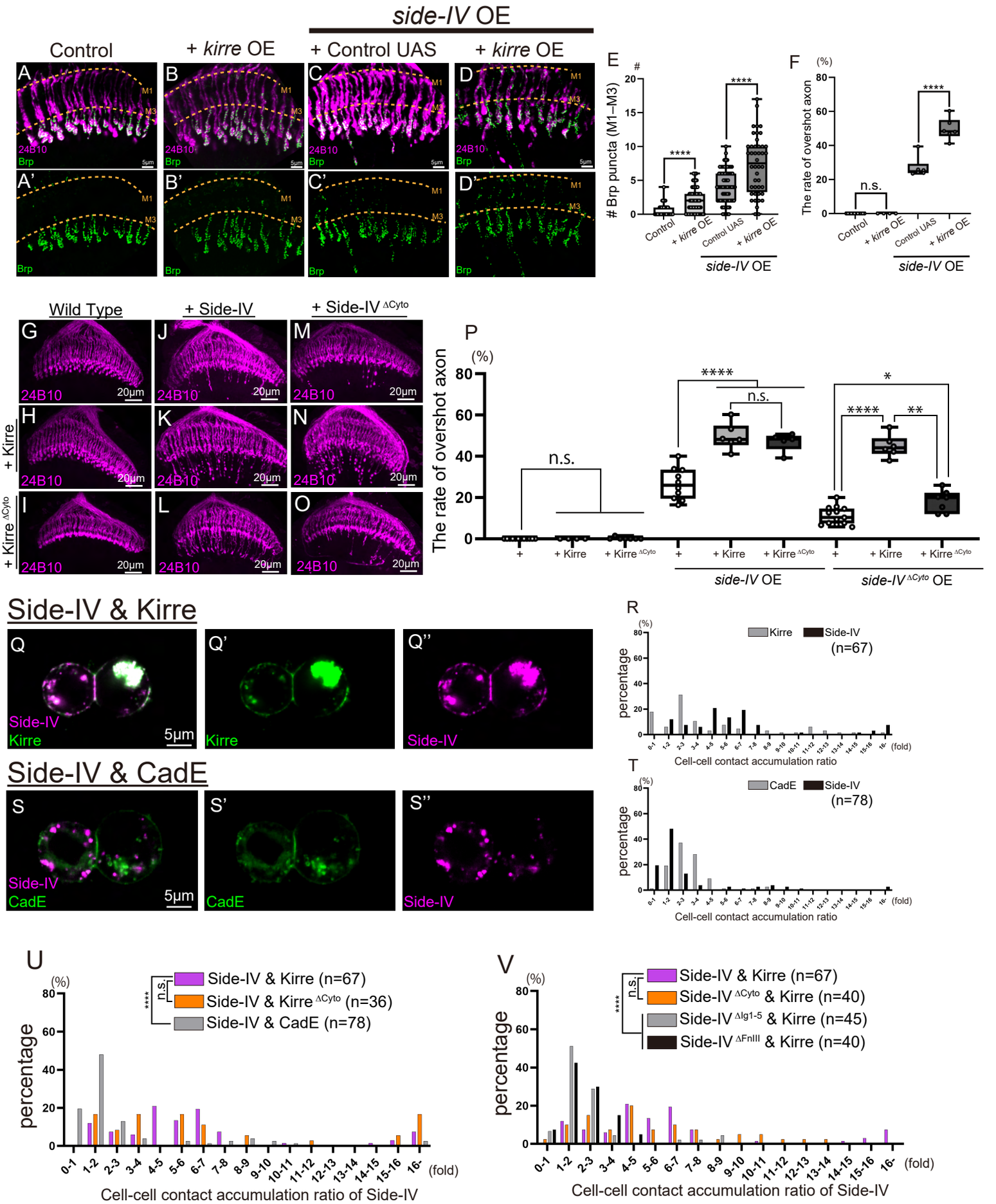
side-IV OE
Control
+ kirre OE
+ Control UAS
+ kirre OE
A
B
C
D
A'
B'
C'
D'
M1
M3
24B10
Brp
5μm
E
Brp puncta (M1–M3)
****
Control
+ kirre OE
Control UAS
+ kirre OE
side-IV OE
F
(%)
The rate of overshot axon
n.s.
****
Wild Type
+ Side-IV
+ Side-IV ΔCyto
G
J
M
H
K
N
I
L
O
+ Kirre
+ Kirre ΔCyto
20μm
P
The rate of overshot axon
n.s.
****
*
**
+
+ Kirre
+ Kirre ΔCyto
side-IV OE
side-IV ΔCyto OE
Side-IV & Kirre
Q
Q'
Q''
Side-IV
Kirre
5μm
R
Kirre
Side-IV
(n=67)
percentage
Cell-cell contact accumulation ratio
(fold)
Side-IV & CadE
S
S'
S''
CadE
T
(n=78)
U
Side-IV & Kirre (n=67)
Side-IV & Kirre ΔCyto (n=36)
Side-IV & CadE (n=78)
Cell-cell contact accumulation ratio of Side-IV
V
Side-IV & Kirre (n=67)
Side-IV ΔCyto & Kirre (n=40)
Side-IV ΔIg1-5 & Kirre (n=45)
Side-IV ΔFnIII & Kirre (n=40)

Figure 3

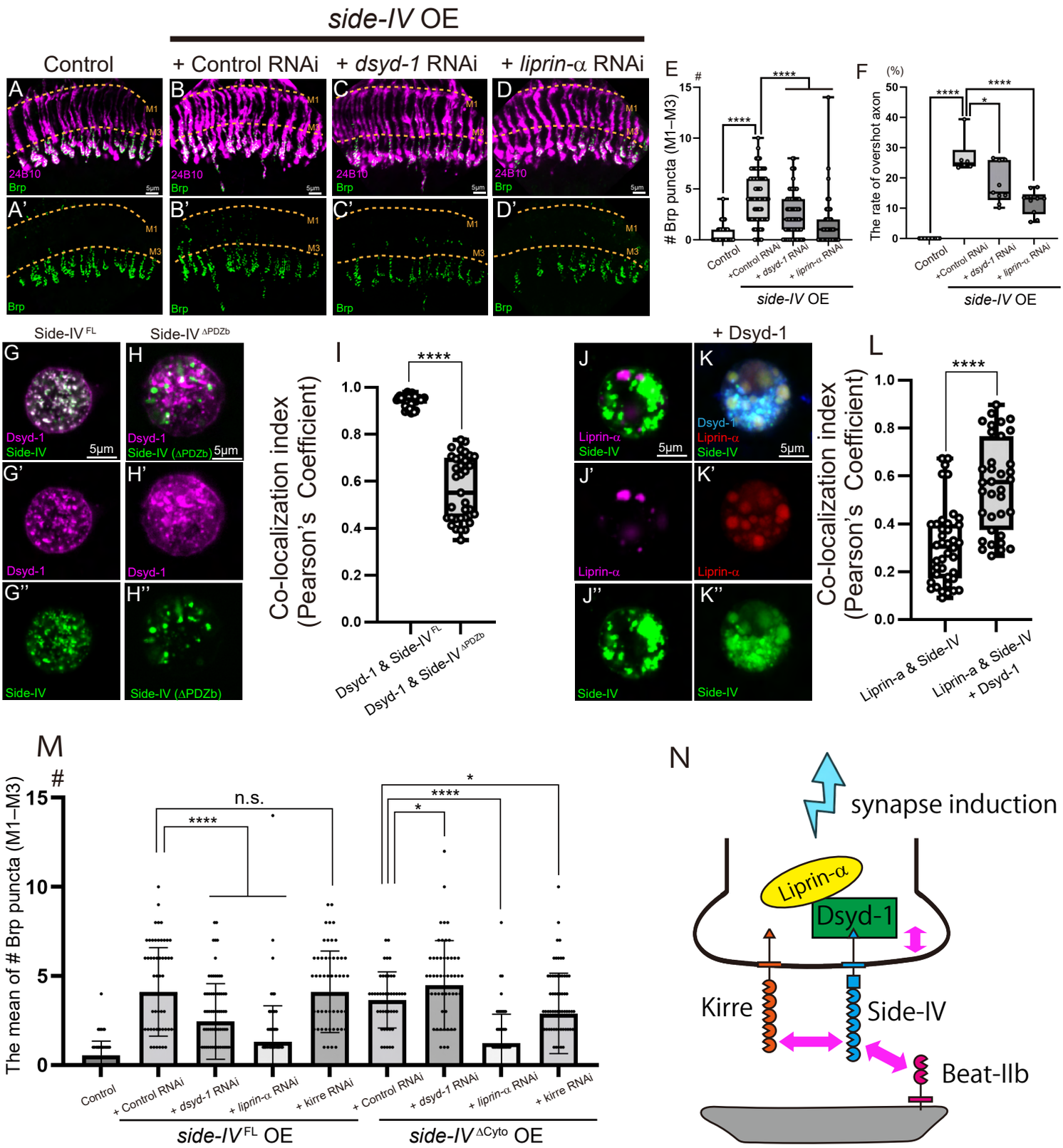
side-IV OE
Control
+ Control RNAi
+ dsyd-1 RNAi
+ liprin-α RNAi
A
B
C
D
A'
B'
C'
D'
M1
M3
24B10
Brp
5μm
E
Brp puncta (M1–M3)
Control
+Control RNAi
+ dsyd-1 RNAi
+ liprin-α RNAi
side-IV OE
F
The rate of overshot axon
(%)
Side-IV FL
Side-IV ΔPDZb
G
H
Dsyd-1
Side-IV
Side-IV (ΔPDZb)
G'
H'
G''
H''
I
Co-localization index
(Pearson's Coefficient)
Dsyd-1 & Side-IV FL
Dsyd-1 & Side-IV ΔPDZb
+ Dsyd-1
J
K
Liprin-α
J'
K'
J''
K''
L
Liprin-a & Side-IV
Liprin-a & Side-IV + Dsyd-1
M
The mean of # Brp puncta (M1–M3)
n.s.
+ kirre RNAi
side-IV FL OE
side-IV ΔCyto OE
N
synapse induction
Liprin-α
Dsyd-1
Kirre
Side-IV
Beat-IIb

Figure 4

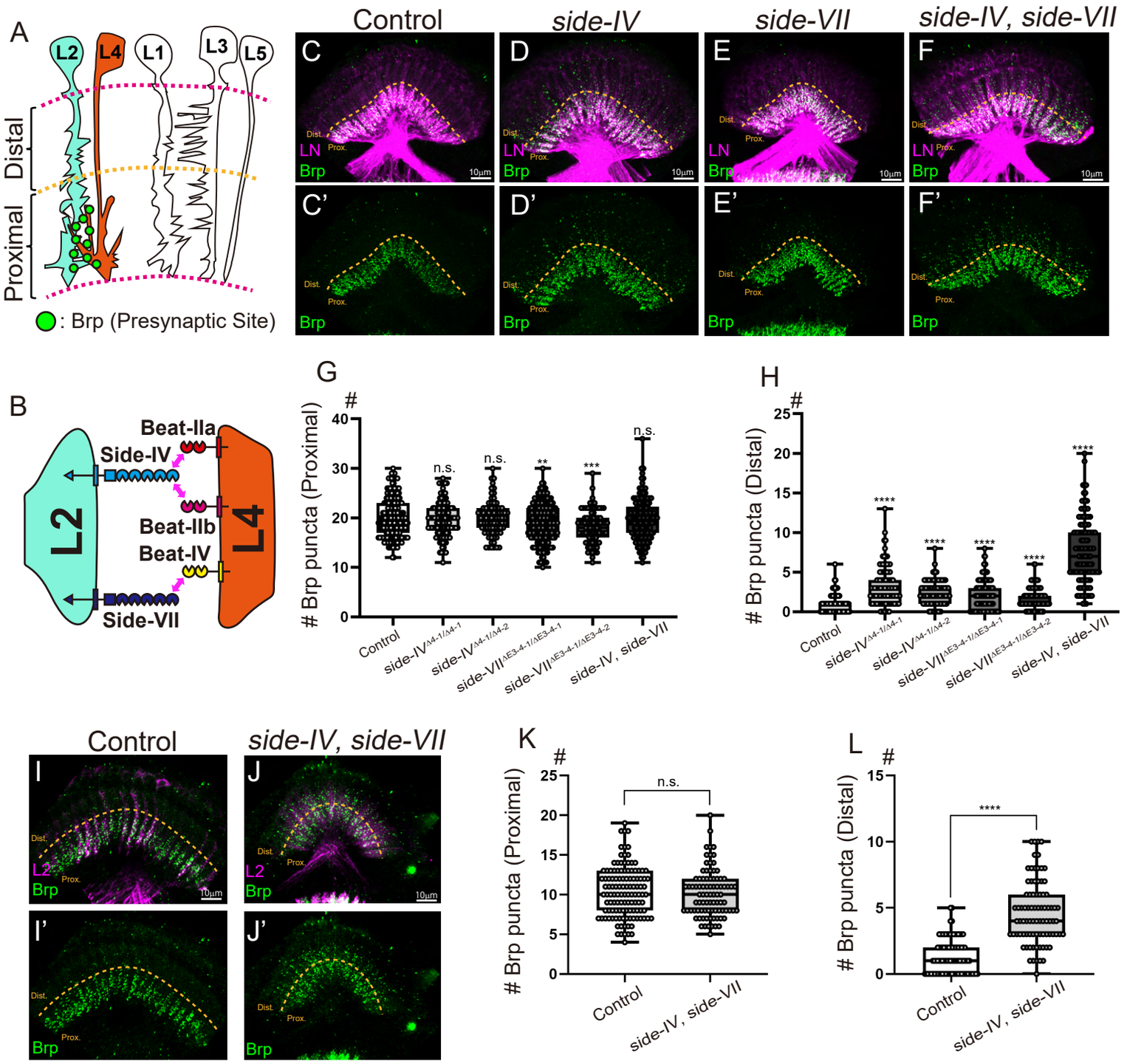
A
L2
L4
L1
L3
L5
Distal
Proximal
: Brp (Presynaptic Site)
Control
side-IV
side-VII
side-IV, side-VII
C
D
E
F
LN
Brp
Dist.
Prox.
10μm
C'
D'
E'
F'
B
Beat-IIa
Side-IV
Beat-IIb
Beat-IV
Side-VII
L2
L4
G
Brp puncta (Proximal)
n.s.
**
***
H
Brp puncta (Distal)
****
Control
side-IV, side-VII
I
J
L2
I'
J'
K
n.s.
L
****

Figure 5

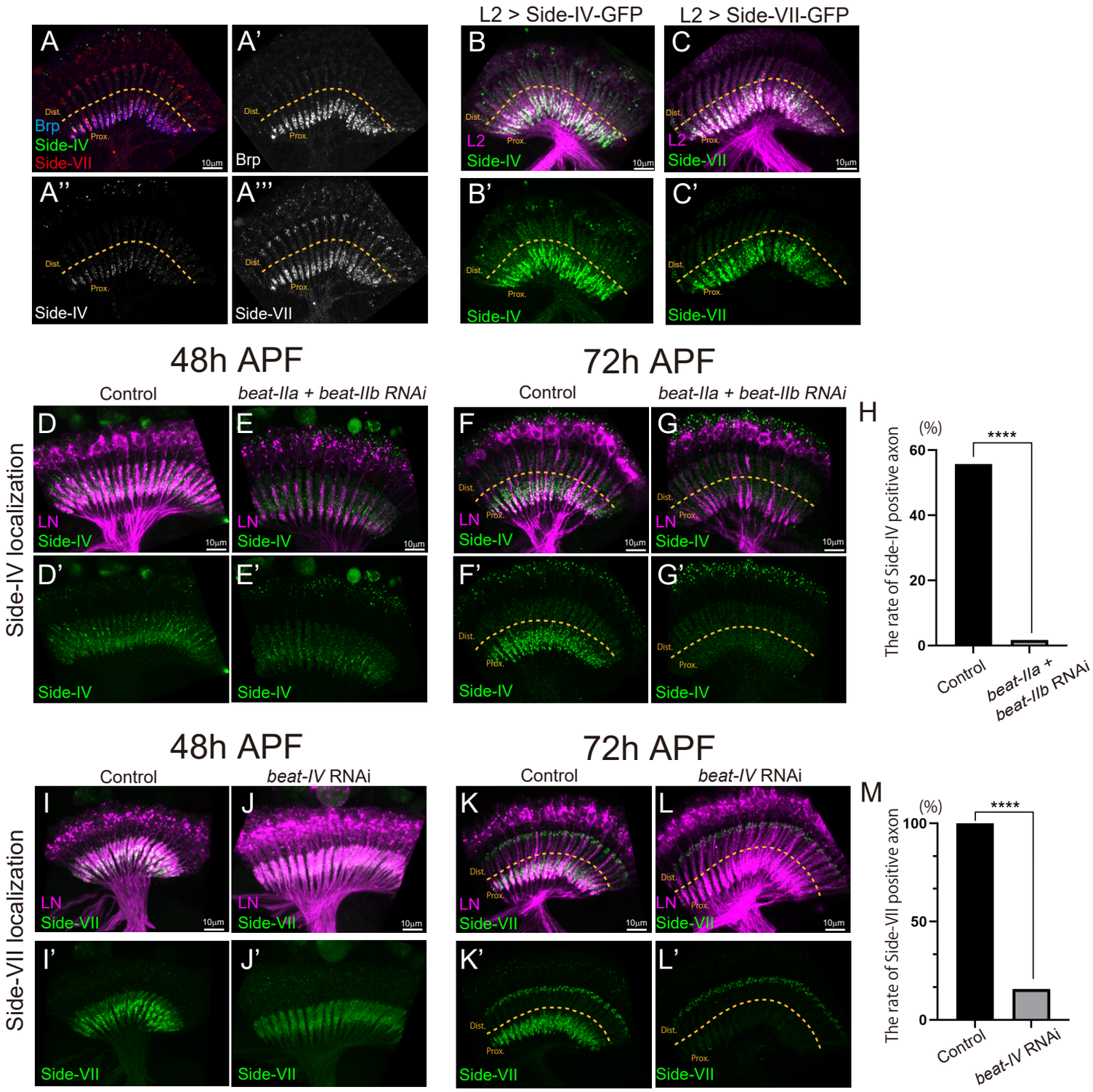
L2 > Side-IV-GFP
L2 > Side-VII-GFP
A
A'
B
C
Brp
Side-IV
Side-VII
L2
A''
A'''
B'
C'
48h APF
72h APF
Control
beat-IIa + beat-IIb RNAi
Side-IV localization
D
E
F
G
LN
D'
E'
F'
G'
H
The rate of Side-IV positive axon
(%)
****
Control
beat-IIa + beat-IIb RNAi
beat-IV RNAi
Side-VII localization
I
J
K
L
I'
J'
K'
L'
M
The rate of Side-VII positive axon
Control
beat-IV RNAi

Figure 6

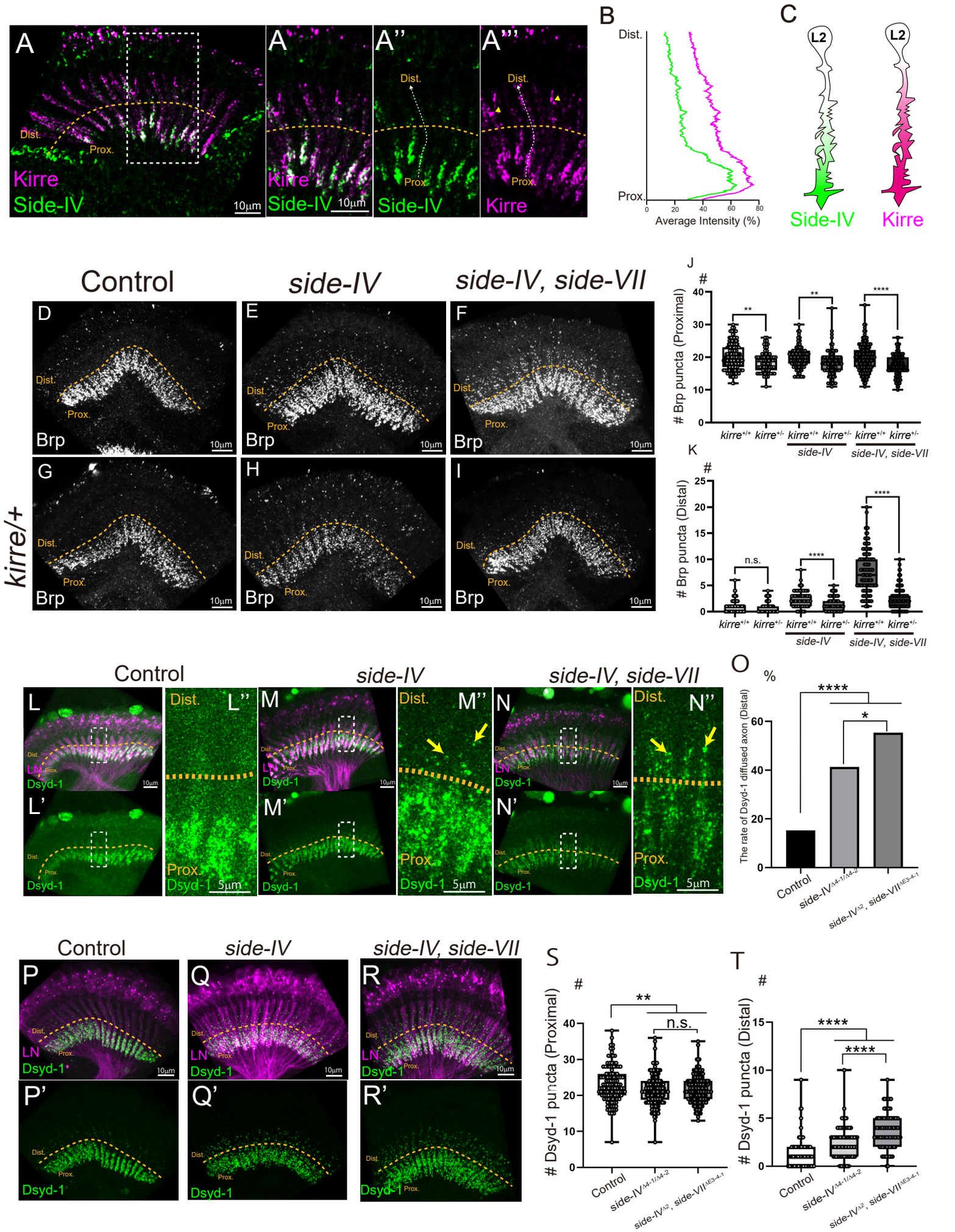
A
Dist.
Prox.
Kirre
Side-IV
10µm
A'
A''
A'''
B
Dist.
Prox.
Average Intensity (%)
C
L2
Side-IV
Kirre
Control
side-IV
side-IV, side-VII
D
E
F
G
H
I
kirre/+
Brp
J
Brp puncta (Proximal)
K
Brp puncta (Distal)
n.s.
kirre+/+
kirre+/-
side-IV
side-IV, side-VII
L
L'
L''
M
M'
M''
N
N'
N''
LN
Dsyd-1
5µm
O
The rate of Dsyd-1 diffused axon (Distal)
Control
side-IV
side-IV, side-VII
P
P'
Q
Q'
R
R'
S
Dsyd-1 puncta (Proximal)
T
Dsyd-1 puncta (Distal)

Figure 7

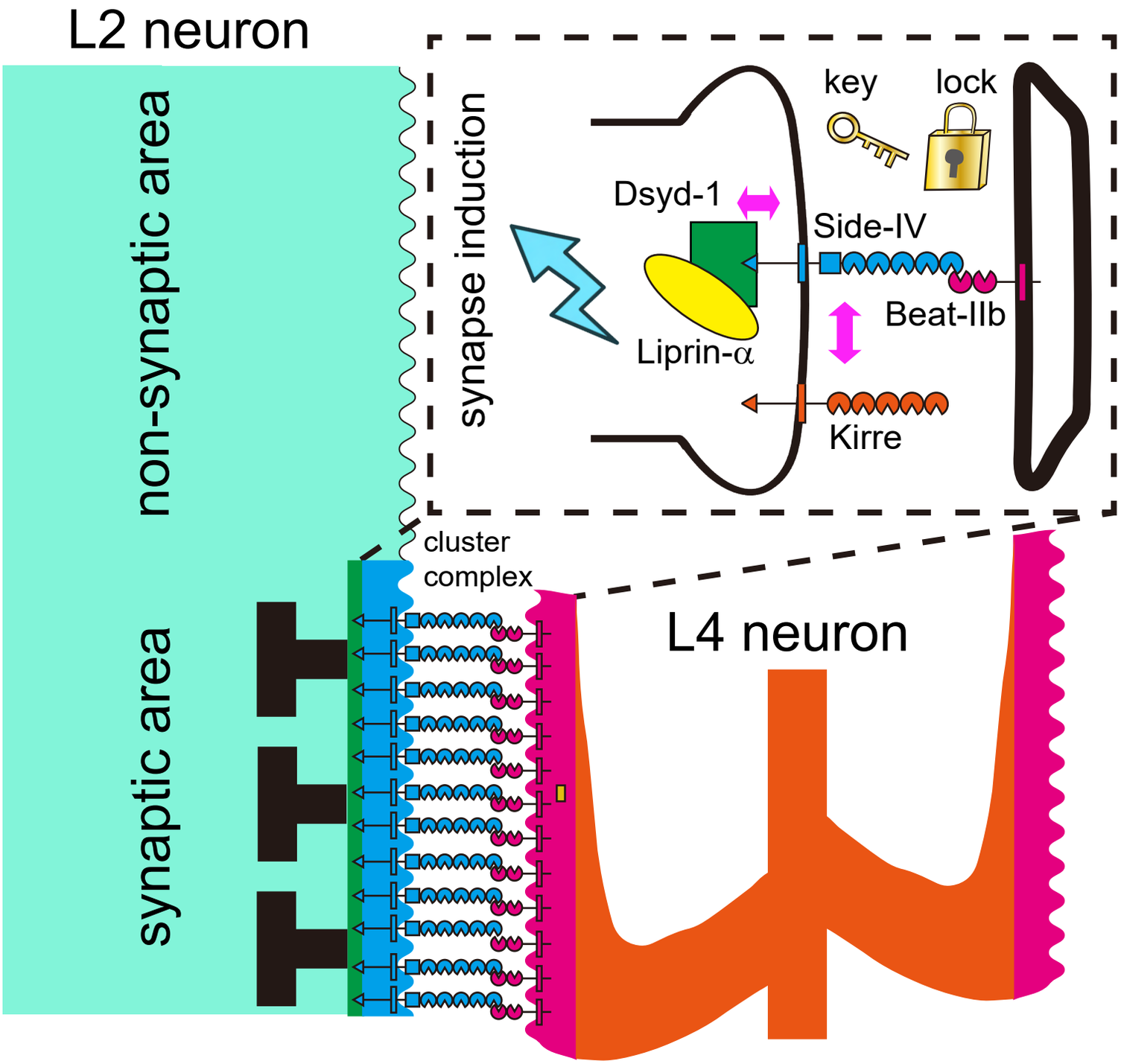
L2 neuron
non-synaptic area
synapse induction
key
lock
Dsyd-1
Side-IV
Beat-IIb
Liprin-α
Kirre
cluster
complex
L4 neuron
synaptic area

Figure 8

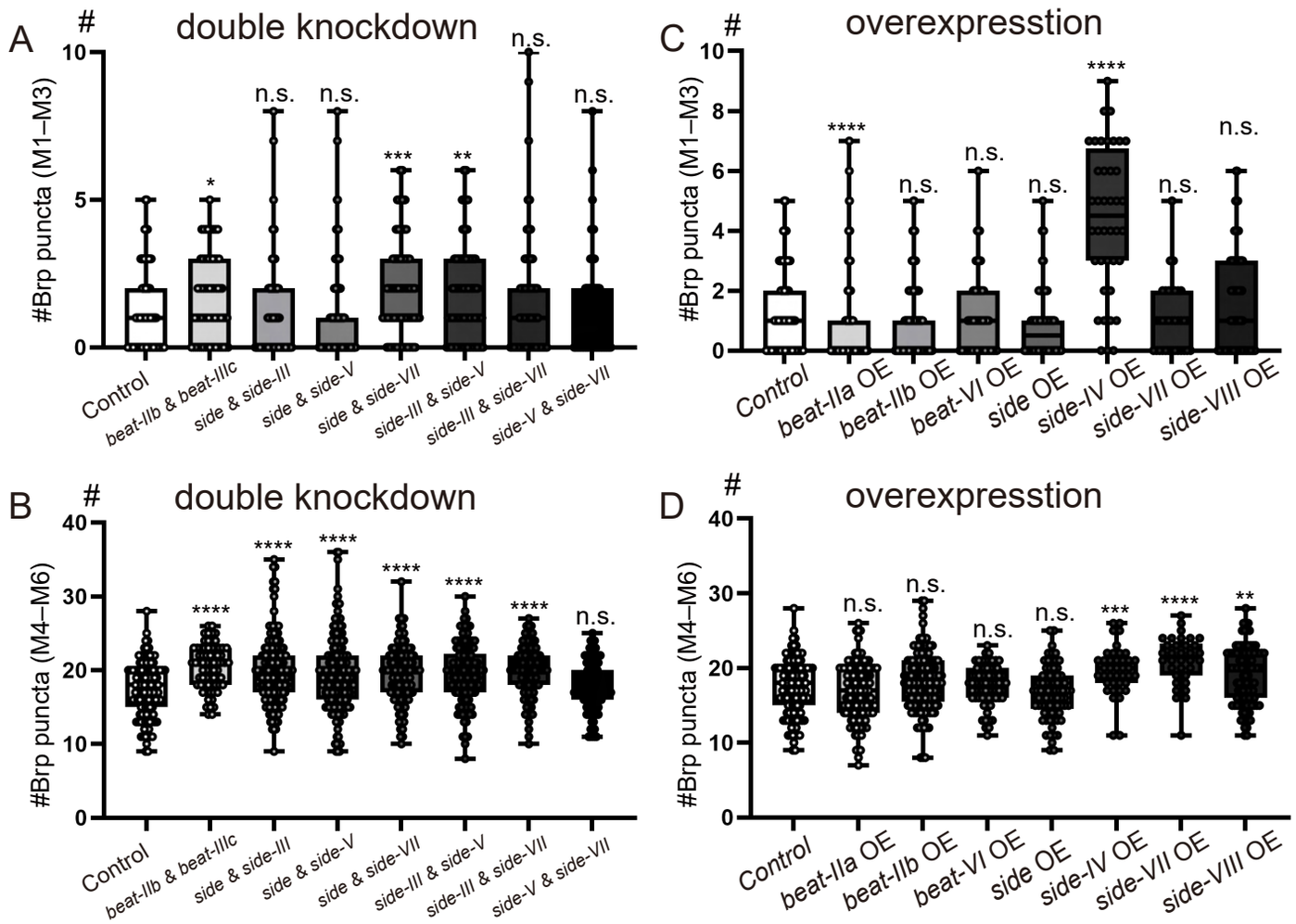
A
double knockdown
#Brp puncta (M1–M3)
Control
beat-IIb & beat-IIIc
side & side-III
side & side-V
side & side-VII
side-III & side-V
side-III & side-VII
side-V & side-VII
C
overexpresstion
#Brp puncta (M1–M3)
Control
beat-IIa OE
beat-IIb OE
beat-VI OE
side OE
side-IV OE
side-VII OE
side-VIII OE
B
double knockdown
#Brp puncta (M4–M6)
D
overexpresstion
#Brp puncta (M4–M6)

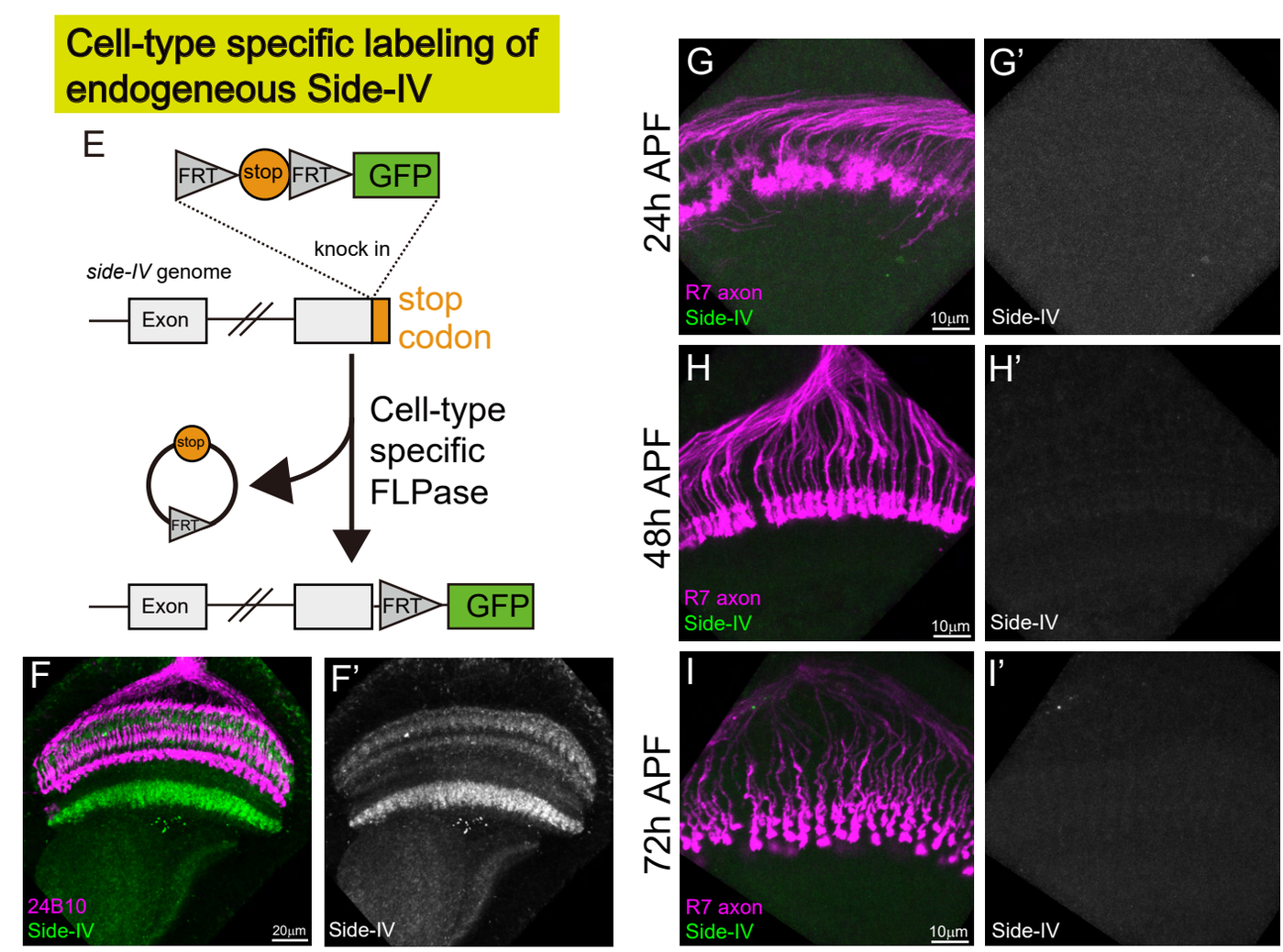
Cell-type specific labeling of endogeneous Side-IV
E
FRT
stop
FRT
GFP
knock in
side-IV genome
Exon
stop codon
Cell-type specific FLPase
stop
FRT
Exon
FRT
GFP
F
24B10
Side-IV
20μm
F'
Side-IV
24h APF
48h APF
72h APF
G
G'
H
H'
I
I'
R7 axon
Side-IV
10μm
Side-IV

Figure S1

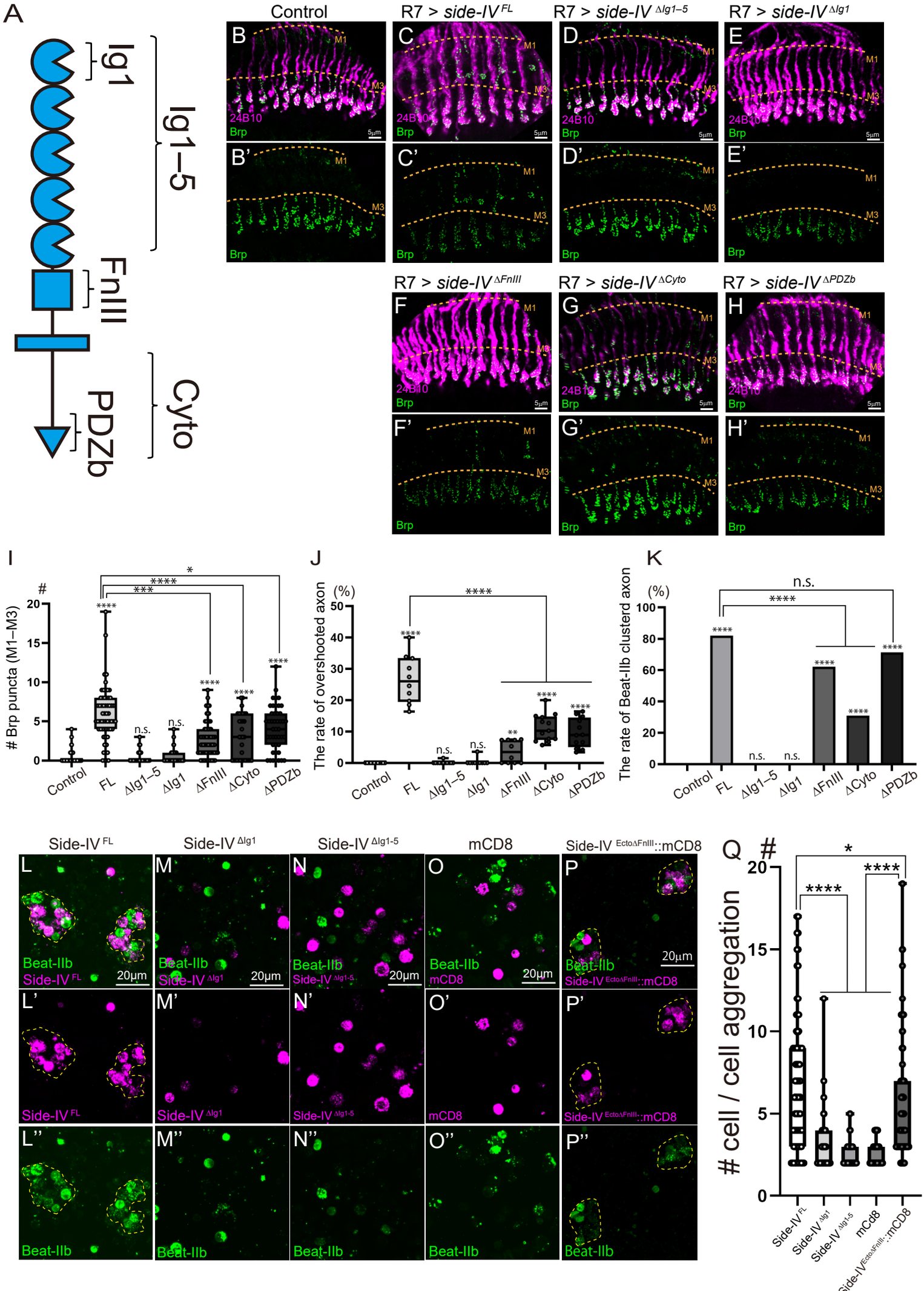
A
Ig1
Ig1–5
FnIII
Cyto
PDZb
Control
R7 > side-IV FL
R7 > side-IV Δlg1–5
R7 > side-IV Δlg1
R7 > side-IV ΔFnIII
R7 > side-IV ΔCyto
R7 > side-IV ΔPDZb
M1
M3
24B10
Brp
5μm
I
Brp puncta (M1–M3)
J
The rate of overshooted axon
(%)
K
The rate of Beat-IIb clustered axon
n.s.
Control
FL
Δlg1–5
Δlg1
ΔFnIII
ΔCyto
ΔPDZb
Side-IV FL
Side-IV Δlg1
Side-IV Δlg1-5
mCD8
Side-IV EctoΔFnIII::mCD8
Beat-IIb
20μm
Q
cell / cell aggregation

Figure S2

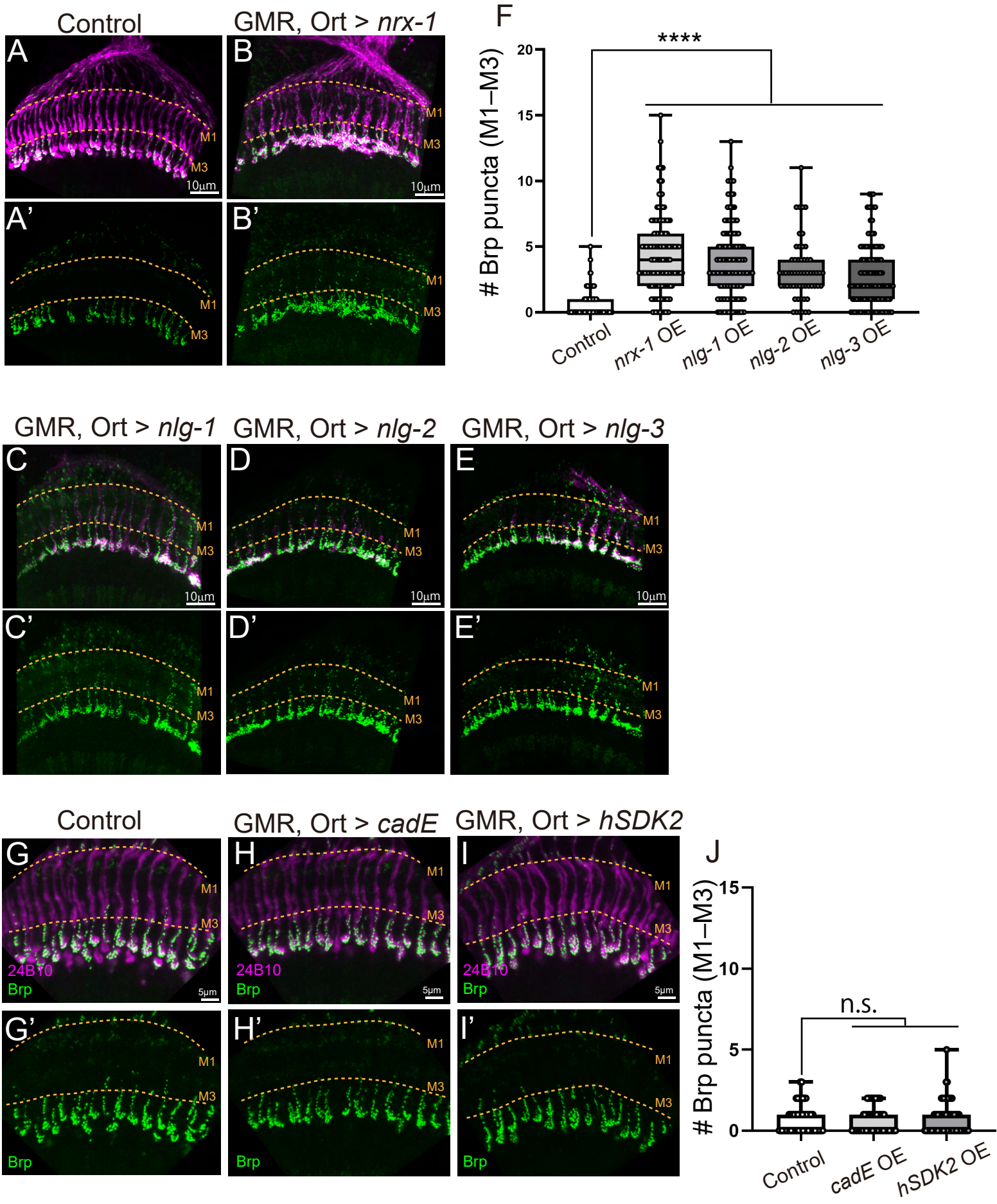
Control
GMR, Ort > nrx-1
A
B
A'
B'
M1
M3
10µm
F
****
Brp puncta (M1–M3)
20
15
10
5
0
Control
nrx-1 OE
nlg-1 OE
nlg-2 OE
nlg-3 OE
GMR, Ort > nlg-1
GMR, Ort > nlg-2
GMR, Ort > nlg-3
C
D
E
C'
D'
E'
Control
GMR, Ort > cadE
GMR, Ort > hSDK2
G
H
I
G'
H'
I'
24B10
Brp
5µm
J
n.s.
Brp puncta (M1–M3)
15
10
5
0
Control
cadE OE
hSDK2 OE

Figure S3

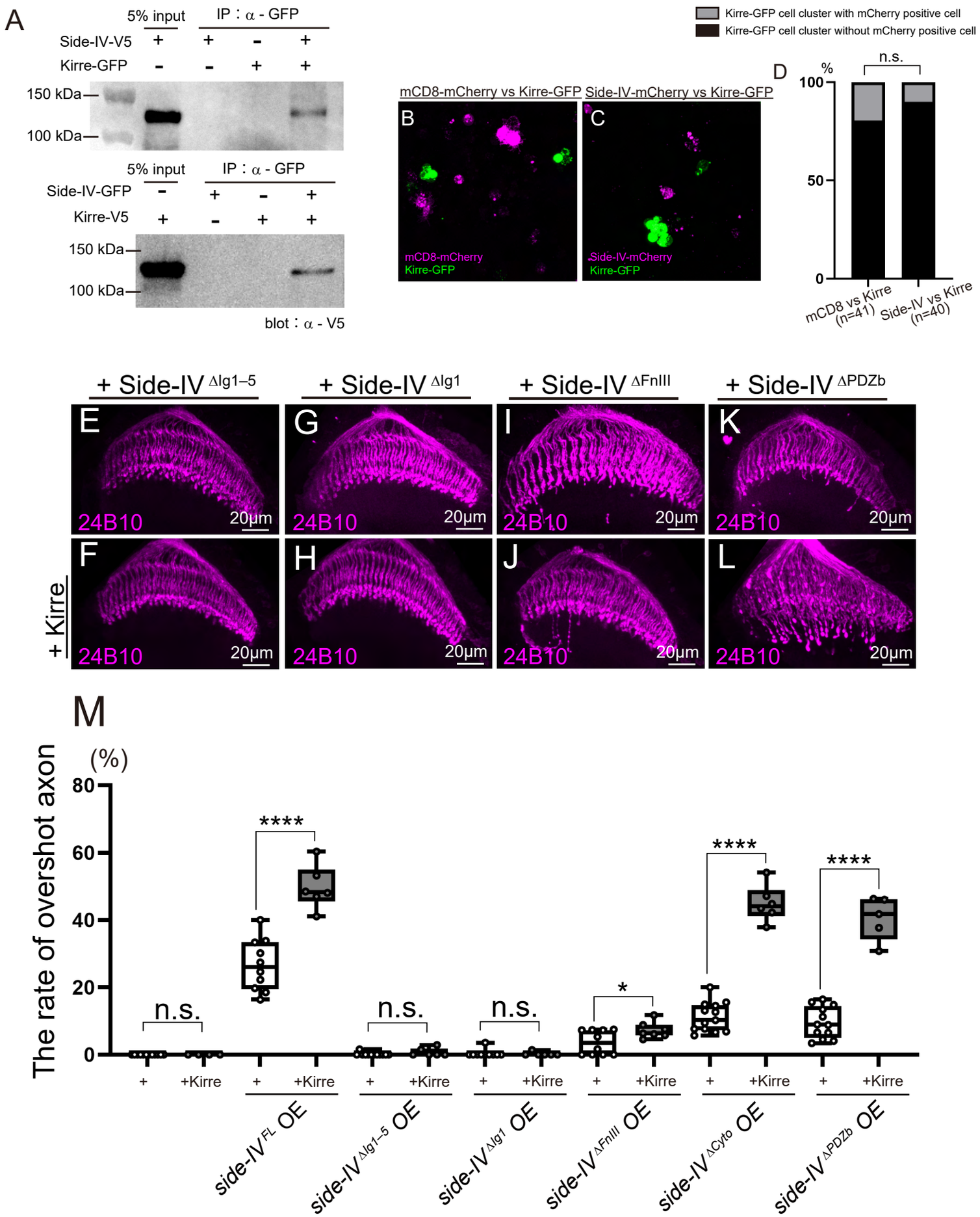
A
5% input
IP : α - GFP
Side-IV-V5
Kirre-GFP
150 kDa
100 kDa
Side-IV-GFP
Kirre-V5
blot : α - V5
Kirre-GFP cell cluster with mCherry positive cell
Kirre-GFP cell cluster without mCherry positive cell
mCD8-mCherry vs Kirre-GFP
Side-IV-mCherry vs Kirre-GFP
B
C
mCD8-mCherry
Kirre-GFP
Side-IV-mCherry
D
n.s.
%
100
50
0
mCD8 vs Kirre (n=41)
Side-IV vs Kirre (n=40)
+ Side-IV ΔIg1–5
+ Side-IV ΔIg1
+ Side-IV ΔFnIII
+ Side-IV ΔPDZb
E
F
G
H
I
J
K
L
24B10
20μm
+ Kirre
M
The rate of overshot axon
(%)
80
60
40
20
0
****
n.s.
*
+
+Kirre
side-IV FL OE
side-IV ΔIg1–5 OE
side-IV ΔIg1 OE
side-IV ΔFnIII OE
side-IV ΔCyto OE
side-IV ΔPDZb OE

Figure S4

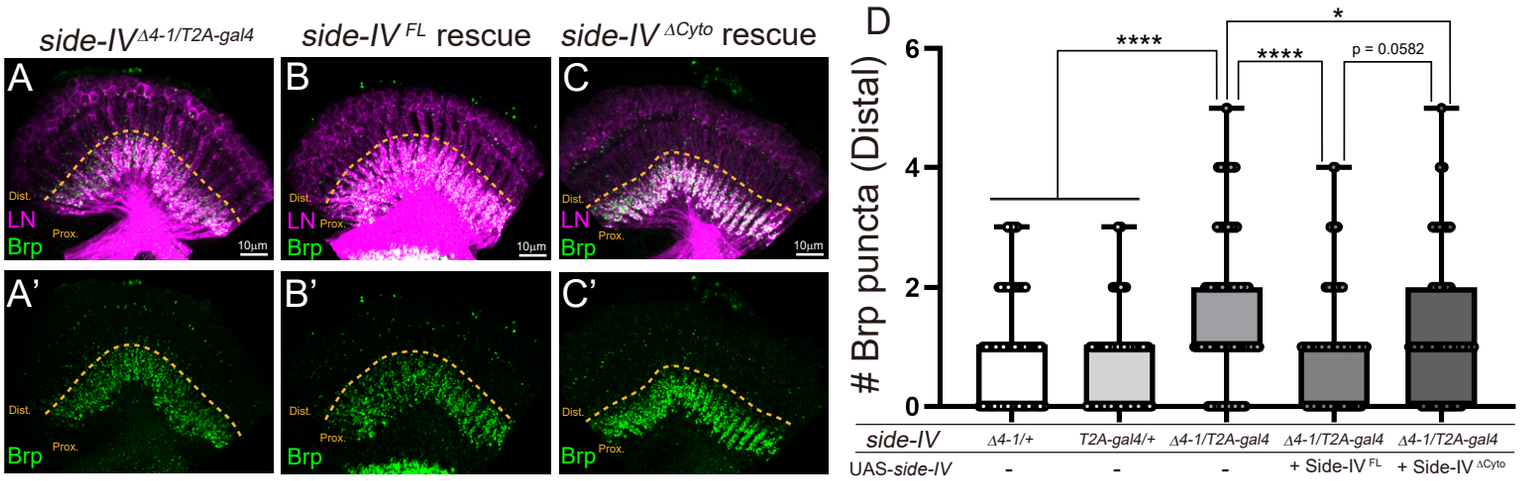
side-IV Δ4-1/T2A-gal4
side-IV FL rescue
side-IV ΔCyto rescue
A
B
C
A'
B'
C'
LN
Brp
Dist.
Prox.
10μm
D
Brp puncta (Distal)
****
*
p = 0.0582
side-IV
Δ4-1/+
T2A-gal4/+
Δ4-1/T2A-gal4
Δ4-1/T2A-gal4
Δ4-1/T2A-gal4
UAS-side-IV
+ Side-IV FL
+ Side-IV ΔCyto

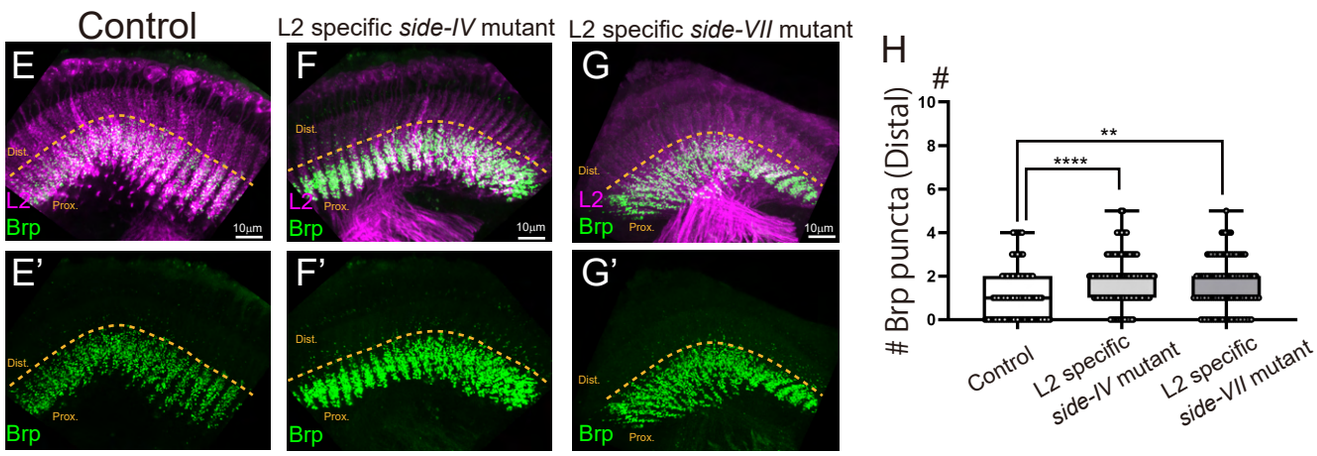
Control
L2 specific side-IV mutant
L2 specific side-VII mutant
E
F
G
E'
F'
G'
L2
Brp
Dist.
Prox.
10μm
H
Brp puncta (Distal)
**
****
Control
L2 specific side-IV mutant
L2 specific side-VII mutant

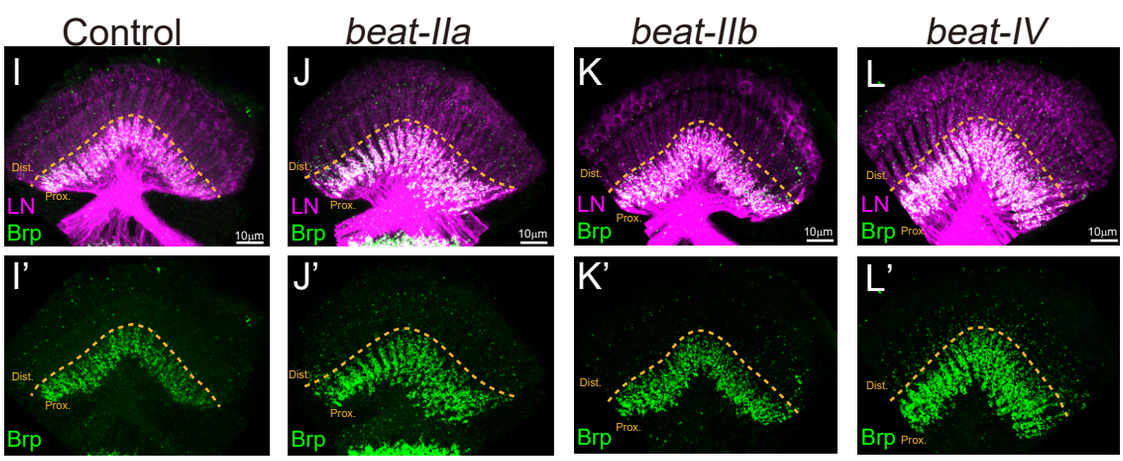
Control
beat-IIa
beat-IIb
beat-IV
I
J
K
L
I'
J'
K'
L'
LN
Brp
Dist.
Prox.
10μm

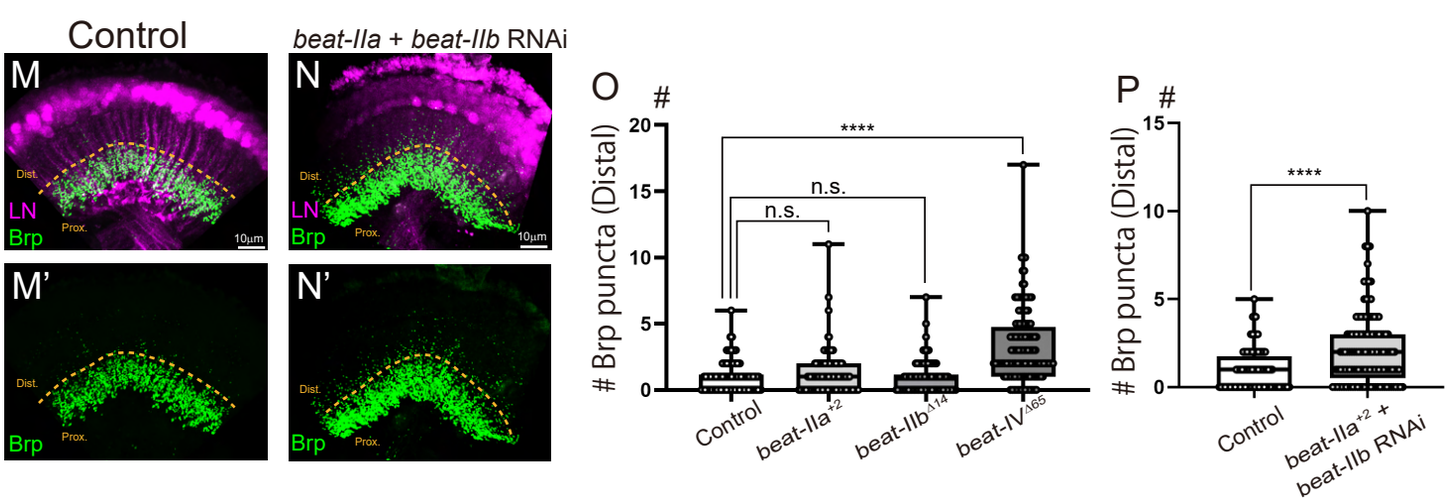
Control
beat-IIa + beat-IIb RNAi
M
N
M'
N'
LN
Brp
Dist.
Prox.
10μm
O
Brp puncta (Distal)
****
n.s.
n.s.
Control
beat-IIa+2
beat-IIb Δ14
beat-IV Δ65
P
Brp puncta (Distal)
****
Control
beat-IIa+2 + beat-IIb RNAi

Figure S5

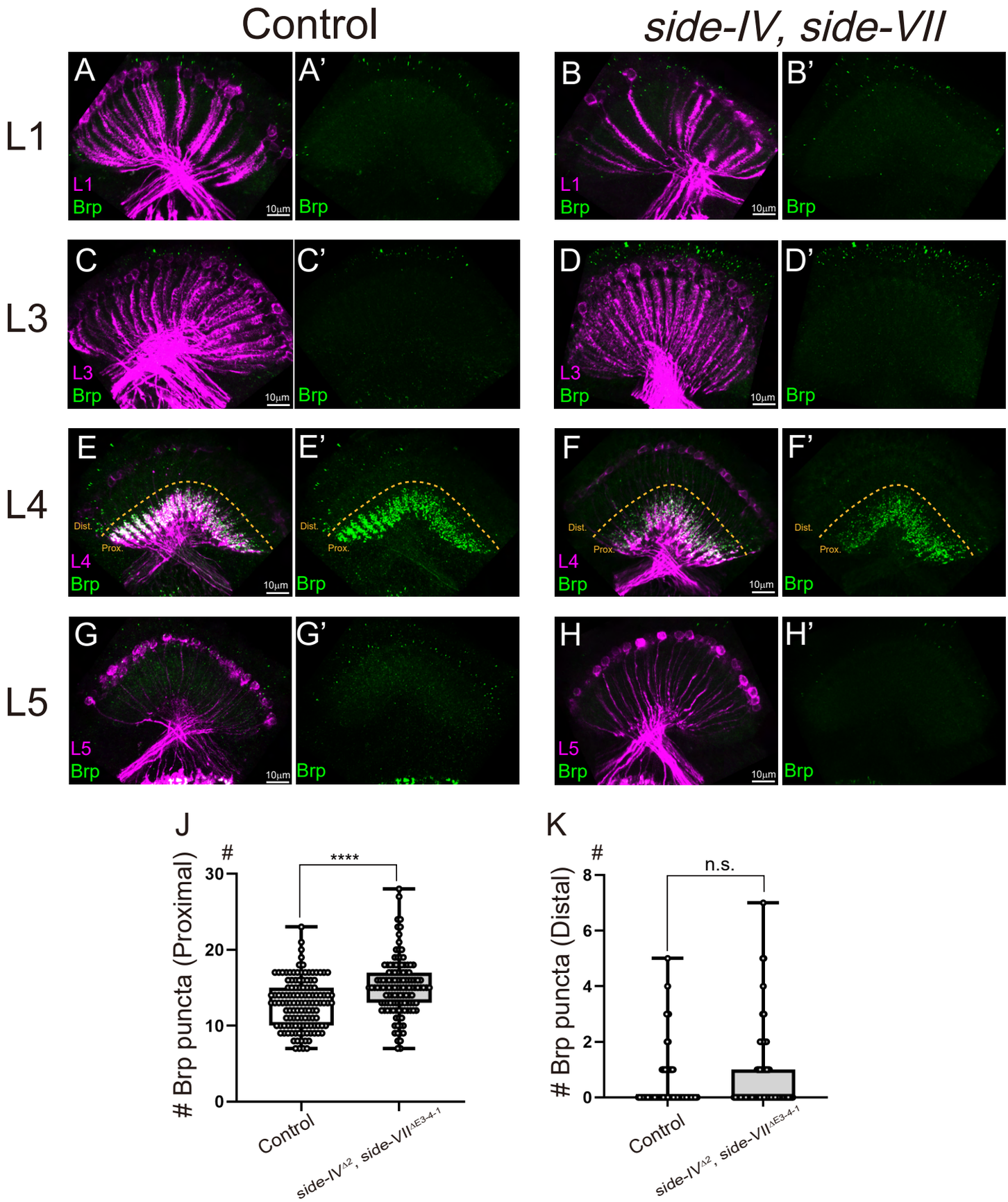
Control
side-IV, side-VII
L1
L3
L4
L5
A
A'
B
B'
C
C'
D
D'
E
E'
F
F'
G
G'
H
H'
L1
L3
L4
L5
Brp
10µm
Dist.
Prox.
J
K
Brp puncta (Proximal)
Brp puncta (Distal)
****
n.s.
Control
side-IV^Δ2, side-VII^ΔE3-4-1

Figure S6

side-IV expresstion in L2 neuron

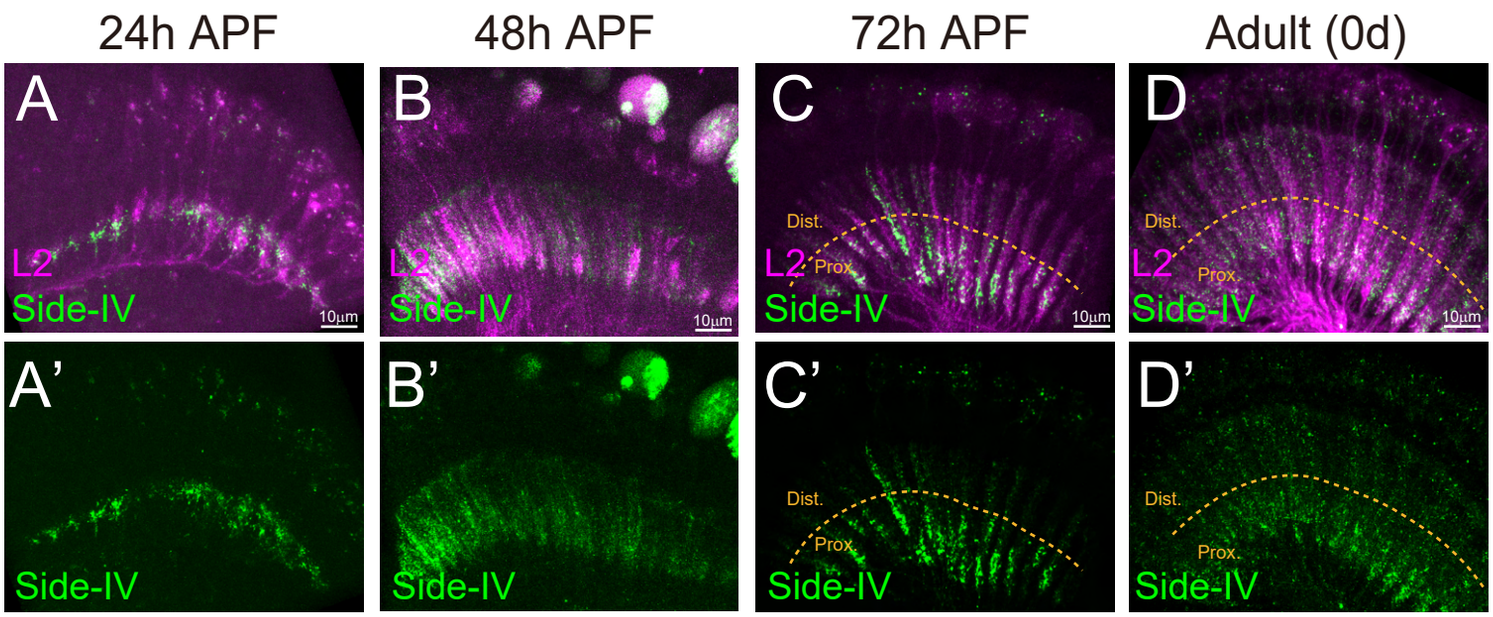

side-VII expresstion in L2 neuron

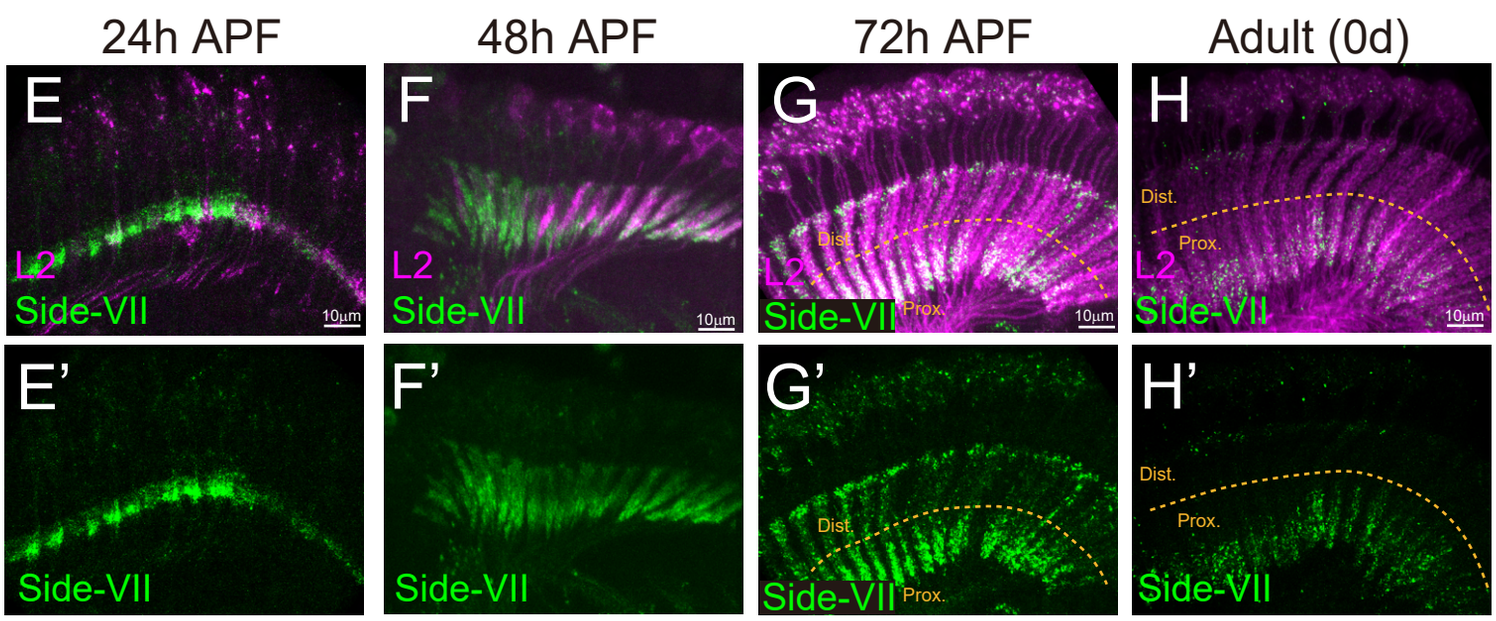

Figure S7

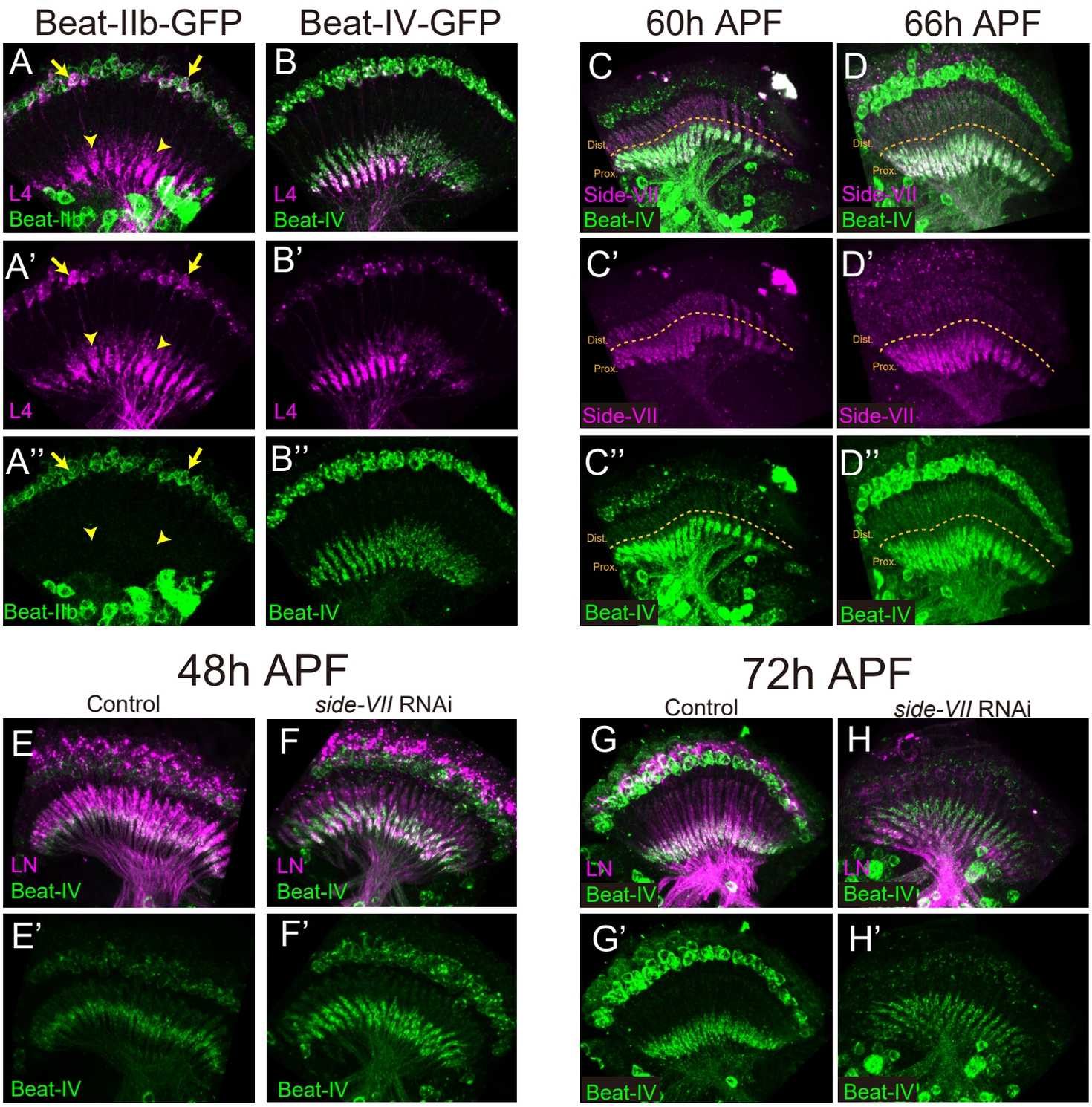
Beat-IIb-GFP
Beat-IV-GFP
60h APF
66h APF
A
L4
Beat-IIb
B
L4
Beat-IV
C
Dist.
Prox.
Side-VII
Beat-IV
D
Dist.
Prox.
Side-VII
Beat-IV
A'
L4
B'
L4
C'
Dist.
Prox.
Side-VII
D'
Dist.
Prox.
Side-VII
A''
Beat-IIb
B''
Beat-IV
C''
Dist.
Prox.
Beat-IV
D''
Dist.
Prox.
Beat-IV
48h APF
Control
side-VII RNAi
72h APF
Control
side-VII RNAi
E
LN
Beat-IV
F
LN
Beat-IV
G
LN
Beat-IV
H
LN
Beat-IV
E'
Beat-IV
F'
Beat-IV
G'
Beat-IV
H'
Beat-IV

Figure S8